

ENTANGLEMENT ENTROPY AND THERMAL PHASE TRANSITIONS FROM CURVATURE SINGULARITIES

Sergio Barbosa^{a *}, Sylvain Fichet^{a †}, Eugenio Megías^{b ‡}, Mariano Quirós^{c §}

^a *CCNH, Universidade Federal do ABC, Santo Andre, 09210-580 SP, Brazil*

^b *Departamento de Física Atómica, Molecular y Nuclear and
Instituto Carlos I de Física Teórica y Computacional,
Universidad de Granada, Avenida de Fuente Nueva s/n, 18071 Granada, Spain*

^c *Institut de Física d'Altes Energies (IFAE) and
The Barcelona Institute of Science and Technology (BIST),
Campus UAB, 08193 Bellaterra, Barcelona, Spain*

Abstract

We study holographic entanglement entropy and revisit thermodynamics and confinement in the dilaton-gravity system. Our analysis focuses on a solvable class of backgrounds that includes AdS and linear dilaton spacetimes as particular cases, with some results extended to general warped metrics. A general lesson is that the behavior of the holographic theory is tied to the bulk curvature singularities. We find that a singular background is confining if and only if *i*) the singularity coincides with a boundary or *ii*) it is the linear dilaton. In the former case, for which the singularity cuts off spacetime, we demonstrate that both entanglement entropy and thermodynamics exhibit a first order phase transition. In the linear dilaton case we find instead that both entanglement entropy and thermal phase transitions are of second order. Additionally, along the process we thoroughly derive the radion effective action at quadratic order.

*sergio.barbosa@aluno.ufabc.edu.br

†sylvain.fichet@gmail.com

‡emegias@ugr.es

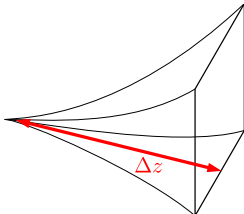
§quiros@ifae.es

Contents

1	Introduction	3
2	Dilaton-Gravity and Singularities	4
2.1	Branes and Holography	5
2.2	Solving the Brane-Dilaton-Gravity System	6
2.3	The \mathcal{M}_ν Spacetime	6
2.4	The Black Hole	8
2.5	On Singularities and Boundaries	8
3	Holographic Confinement	10
3.1	The Holographic Wilson Loop	10
3.2	String Shape in Dilatonic Background	11
3.3	Confinement	13
3.4	Comparison to Asymptotically AdS backgrounds	14
4	Holographic Entanglement Entropy	15
4.1	Elementary Properties	15
4.2	Phase Transition and Boundaries	17
4.3	Smooth Surfaces in the \mathcal{M}_ν^- background	20
4.4	Holographic Entanglement Entropy in the \mathcal{M}_ν^- background	22
5	Stability and the Radion Effective Action	23
5.1	The Effective Potential	23
5.2	The Radion	24
5.3	Radion Mass from the On-Shell Action	25
6	Holographic Thermal Phase Transitions	27
6.1	Thermodynamics on the Brane	28
6.2	Phase Transitions	29
6.3	Discussion	31
6.4	Instability from Big Black Holes	32
7	Summary	33
A	Derivation of Property (2.18)	36
B	Minimal Surfaces and Geodesics	36

1 Introduction

Some classes of holographic spacetimes beyond pure Anti-de Sitter feature a curvature singularity. The singularity may be either at finite or infinite conformal distance from the boundary on which the lower-dimensional dual theory is computed. That is, we have schematically



with Δz finite or not. In this paper we argue that this simple distinction controls key properties of the dual theory, including the behavior of entanglement entropy, thermal phase transitions, and confinement.

The phenomenon of confinement remains an unsolved puzzle of QFT at strong coupling. One route to understand confinement is to describe it holographically, using a gauge-gravity duality that may potentially encode the strong dynamics in a gravitational higher-dimensional spacetime. While the most precise and well-established duality of this kind is the AdS/CFT correspondence [1–4], CFTs cannot confine since they have no scale. The holographic view of confinement, if it exists, must come from a different, less symmetric spacetime beyond AdS, that allows for the emergence of a confinement scale.

The gauge-gravity correspondence being an offspring of string theory, natural candidates for holography beyond AdS are motivated by non-critical string-inspired models [5–9]. The low-energy effective action in such models describes spacetime augmented with an extra scalar field, the dilaton. Going beyond AdS/CFT naturally leads to exploring the properties of the dilaton-gravity system.

One reason to expect that dilatonic backgrounds are holographic is the existence of a known example: the linear dilaton spacetime, whose corresponding dual theory is little string theory (LST).¹ More generally it is widely accepted that a (less predictive) holographic principle formulated in terms of information content applies to any spacetime [36–40]. These are strong motivations to investigate the holography of the dilaton-gravity system, including the holographic version of confinement.²

Hints that certain non-AdS spacetime backgrounds describe confining dynamics have been gradually gathered, using holographic descriptions of the quark-antiquark potential [9, 48–56], of thermal phase transitions [57–64], and of entanglement entropy [65–76]. Such phenomena can be viewed as probes that test whether a background is confining, based on the broad qualitative features expected from confining theories.

While a number of studies of holographic entanglement entropy — as a probe of confinement — have been done in stringy and supersymmetric backgrounds (see [65–74, 76–80]),

¹See [10–12] for LST reviews, [13–27] for formal holographic aspects of the linear dilaton background, and [12, 28–35] for field theoretical studies of the LD background and related phenomenological developments.

²See e.g. [8, 9, 41–47] for related studies of the dilaton-gravity system.

holographic entanglement has not been studied in the simple dilaton-gravity system, to the best of our knowledge, apart from a brief case study [81]. One goal of this paper is to fill this gap.

Another objective of this study is to elucidate the relationship between curvature singularities and confinement. These singularities, induced by the backreaction of the metric on the dilaton vacuum expectation value (vev), are prevalent in dilaton-gravity models. Here, we will categorize the singularities in terms of conformal distance to the brane, a distinction that we will show to be linked to the confining nature of the background.

A third objective of this paper is to provide a unified view and a simple set of intuitions for the various probes of confinement, that can be applied to e.g. asymptotically AdS backgrounds. Here we compute all these phenomena in a class of non-asymptotically AdS backgrounds (previously used in [82], see also [83–86]) that retains the essence of the features we want to highlight. This class of backgrounds has a single continuous parameter and contains both the linear dilaton and AdS as particular cases.

Our study is structured as follows. In section 2 we define the D -dimensional dilaton-gravity system of our interest, and classify its curvature singularities. In section 3 we analyze the string-based notion of confinement in this background, developing intuitions that also apply to asymptotically-AdS backgrounds. In section 4 we compute the holographic entanglement entropy of a $(D - 2)$ -strip localized on the boundary, including finite temperature corrections. In section 5 we compute the radion effective action. At zero temperature this controls the stability of the brane-dilaton system. At finite temperature the radion effective action gives access to the free energy. We explore the structure of phase transitions in section 6. Our findings are summarized in section 7. Appendix A contains a derivation of a property used in the analysis of metric zeros.

2 Dilaton-Gravity and Singularities

We consider a spacetime with $D = d + 1$ dimensions. The action of the D -dimensional dilaton-gravity system in the Einstein frame is

$$\begin{aligned} \mathcal{S} = & \int d^D x \sqrt{g} \left(\frac{M_D^{D-2}}{2} {}^{(D)}R - \frac{1}{2} (\partial_M \phi)^2 - V(\phi) \right) \\ & - \int_{\text{brane}} d^d x \sqrt{\bar{g}} \left(V_b(\phi_b) + \Lambda_b - M_D^{D-2} K \right) + \mathcal{S}_{\text{matter}}, \end{aligned} \quad (2.1)$$

where ${}^{(D)}R$ is the scalar curvature, ϕ the dilaton field, M_D the fundamental D -dimensional Planck scale, and g_{MN} the bulk metric with mostly plus signature. $\mathcal{S}_{\text{matter}}$ encodes the quantum fields living on this background.

The spacetime supports a $(d - 1)$ -brane, with induced metric $\bar{g}_{\mu\nu}$, tension Λ_b and a localized potential $V_b(\phi_b)$, where $\phi_b \equiv \phi|_{\text{brane}}$ stands for the value of the dilaton field at the brane. K is the extrinsic curvature that appears in the Gibbons-Hawking-York (GHY) boundary term. The $V_b(\phi_b)$ potential stabilizes ϕ_b to the vacuum expectation value (vev) $\langle \phi_b \rangle \equiv v_b$, which determines completely the background.

The $V_b(\phi_b)$ potential is assumed to satisfy a mild condition, specified further below, that ensures stability of spacetime [82]. This assumption and the fact that $V_b(\phi_b)$ stabilizes ϕ_b are sufficient in the scope of our study, hence the explicit form of $V_b(\phi_b)$ does not need to be further specified. We use the convention $V_b(v_b) = 0$ without loss of generality.

The most general metric ansatz we consider is the warped foliation

$$ds^2 = g_{MN} dx^M dx^N = g_{xx}(r) \eta_{\mu\nu} dx^\mu dx^\nu + g_{rr}(r) dr^2, \quad (2.2)$$

with arbitrary g_{xx} , g_{rr} coefficients. Some of our results will be derived with this general metric, using sometimes monotonicity assumptions involving the metric coefficients.

2.1 Branes and Holography

The stabilization of the dilaton-gravity system involves a brane. We will see throughout this paper that the dual holographic theory is naturally defined on this brane.

2.1.1 Branes

From the low-energy viewpoint, a brane is simply an infinitely thin hypersurface living in the higher dimensional spacetime and on which operators and degrees of freedom can be localized [87–89].³

All fields, including the graviton, satisfy boundary conditions on the brane. At low-energies, the brane may be thought as a defect with spacetime existing on both sides. In such a case, the dynamics of the brane can be obtained using the Codacci equation [93] or equivalently Israel’s junction condition [94]. These relate the extrinsic curvatures on both sides of the brane to the brane-localized stress tensor, $\tau_{\mu\nu}$ [27]. One has

$$[K_{\mu\nu}] \equiv K_{\mu\nu}^+ - K_{\mu\nu}^- = -\frac{1}{M_D^{D-1}} \left(S_{\mu\nu} - \frac{1}{D-2} \bar{g}_{\mu\nu} S \right), \quad (2.3)$$

where $S_{\mu\nu} = -\Lambda_b \bar{g}_{\mu\nu} + \tau_{\mu\nu}$. A particular case is when both sides are simply the mirror of each other, i.e. related by a Z_2 symmetry, so that $K_{\mu\nu}^+ = -K_{\mu\nu}^-$ (as by definition $K_{\mu\nu}$ is Z_2 -odd) and then $K_{\mu\nu}^\pm = \pm \frac{1}{2} [K_{\mu\nu}]$. This is the “ Z_2 -orbifold” picture used in braneworld computations such as [93].

Equivalently, the brane may be thought of as a wall beyond which spacetime ends instead of being “mirrored”. This is called an end-of-the-world (EOW) brane. In this case, the dynamics of the brane is determined by letting the metric be dynamical on the brane. This produces a Neumann-type boundary condition that takes precisely the form of (2.3) with zero $K_{\mu\nu}$ on the empty side. This means that for the \mathcal{M}_ν^- space that will be introduced in Sec. 2.3, one has $K_{\mu\nu}^+ = 0$ so that $K_{\mu\nu}^- = -[K_{\mu\nu}]$ with differs by a factor of 2 from the result within the Z_2 -orbifold convention.⁴ The EOW picture is equivalent to the Z_2 -orbifold picture, and one can be translated into the other just paying attention to

³From the UV viewpoint branes may be viewed as solitons. Similar objects naturally appear in string theory as D-branes, which are dynamical objects with quantum properties [90, 91]. Black brane solutions also arise in the supergravity limit of string theories [1, 92].

⁴For the \mathcal{M}_ν^+ space, one would have instead $K_{\mu\nu}^- = 0$ and $K_{\mu\nu}^+ = [K_{\mu\nu}]$.

some factors of 2 related to the Z_2 mirroring. In this paper we use the Z_2 -orbifold picture, which is needed in sections 5 and 6.

2.1.2 Holography on the Brane

The holographic theory is defined by integrating out the bulk degrees of freedom, providing an effective d -dimensional theory supported on the brane. In the context of dilaton gravity, the existence of the brane is mandatory in the sense that it stabilizes the dilaton-gravity system and fixes the physical scale. The brane can optionally be thought as a regulator and be sent to a conformal boundary to recover the asymptotic approach to holography.

The advantage of our approach is that well-understood braneworld-like computation techniques such as those from [93, 95, 96] can be applied. Non-trivial consistency checks of our solutions made within this formalism can be found in [27, 34, 82].

2.2 Solving the Brane-Dilaton-Gravity System

The bulk field equations are

$$0 = {}^{(D)}R_{MN} - \frac{1}{2}g_{MN}{}^{(D)}R - \frac{1}{M_D^{D-2}}\partial_M\phi\partial_N\phi + \frac{1}{2M_D^{D-2}}g_{MN}(\partial_A\phi)^2 + \frac{1}{M_D^{D-2}}g_{MN}V(\phi), \quad (2.4)$$

$$0 = \frac{1}{\sqrt{g}}\partial_M(\sqrt{g}g^{MN}\partial_N\phi) - \frac{\partial V}{\partial\phi}. \quad (2.5)$$

In addition, the brane-localized terms in the action induce some boundary conditions at the brane, that are of the form $[K_{\mu\nu}] \equiv K_{\mu\nu}^+ - K_{\mu\nu}^- = \mathcal{F}(\bar{g}_{\mu\nu}, \phi_b)$ and $[\phi'] \equiv \phi'_+ - \phi'_- = \mathcal{G}(\bar{g}_{\mu\nu}, \phi_b)$ (see Eq. (2.3)) [97]. The solutions to the field equations have integration constants that need careful analysis: some are gauge redundancies, other are physically meaningful. Some integration constants are fixed by the boundary conditions at the brane. On the other hand, a combination of integration constants is fixed by the requirement that the vev does not change with the brane location, $\frac{\partial v_b}{\partial r_b} = 0$ [27], this being a natural consequence of the fact that the $V_b(\phi_b)$ potential is independent on the brane location. We refer to [27] for a detailed discussion.

2.3 The \mathcal{M}_ν Spacetime

We introduce the reduced bulk potential $V(\phi) \equiv (D-2)M_D^{D-2}\bar{V}(\bar{\phi})$ and the reduced dilaton field $\phi \equiv \sqrt{(D-2)M_D^{D-2}}\bar{\phi}$. \bar{V} has mass dimension 2, while $\bar{\phi}$ is dimensionless. The \mathcal{M}_ν spacetime used in this work is defined by setting the reduced bulk potential to

$$\bar{V}(\bar{\phi}) = -\frac{1}{2}(D-1-\nu^2)k^2 e^{2\nu\bar{\phi}}. \quad (2.6)$$

Here ν is a real parameter that we take positive without loss of generality.

We assume that the brane is flat, i.e. r_b does not depend on the space coordinates. While the brane could evolve in time, as studied in [27, 82], see e.g. [95, 96, 98] for AdS, here we consider a static spacetime where r_b is constant in x^μ .

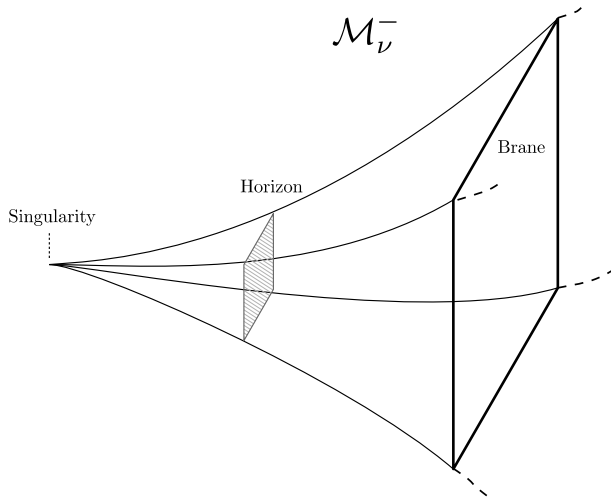


Figure 1. Sketch of the \mathcal{M}_ν^- spacetime. The curvature singularity can be hidden behind a horizon for $\nu < \sqrt{D-1}$.

In the absence of a black hole horizon, the solutions to the field equations following from the action (2.1) are found to be [82]

$$ds_{\nu, r_b}^2 = \left(\frac{r}{L}\right)^2 \eta_{\mu\nu} dx^\mu dx^\nu + \left(\frac{r}{r_b}\right)^{2\nu^2} \frac{1}{(\eta r)^2} dr^2, \quad (2.7)$$

$$\bar{\phi}(r) = \bar{\phi}_b - \nu \log\left(\frac{r}{r_b}\right), \quad (2.8)$$

with $r \in \mathbb{R}_+$. L is a constant with dimension of length. In (2.8), $\bar{\phi}_b = \frac{1}{\sqrt{(D-2)M_D^{D-2}}} \phi_b$ is the value of the reduced dilaton field on the brane. The dilaton vev and the other parameters of the metric combine to form the physical scale $\eta \equiv k e^{\nu \bar{\phi}_b}$, that appears in observable quantities.

The brane at $r = r_b$ partitions \mathcal{M}_ν into two regions

$$\mathcal{M}_\nu^- = \mathcal{M}_\nu|_{r \in (0, r_b]}, \quad \mathcal{M}_\nu^+ = \mathcal{M}_\nu|_{r \in [r_b, \infty)}. \quad (2.9)$$

Our focus in this work is the \mathcal{M}_ν^- space. We mention sometimes \mathcal{M}_ν^+ for comparison.

Conformal frame

We sometimes use conformal coordinates throughout this work. For any $\nu \neq 1$ these are defined as

$$z = \frac{L}{\eta r_b} \frac{1}{|\nu^2 - 1|} \left(\frac{r}{r_b}\right)^{\nu^2 - 1}, \quad \nu \neq 1, \quad (2.10)$$

with the domain $z \in \mathbb{R}_+$. The metric in conformal coordinates reads

$$ds_{\nu, r_b}^2 = \left(\frac{r_b}{L}\right)^{\frac{2\nu^2}{\nu^2 - 1}} (|\nu^2 - 1| \eta z)^{\frac{2}{\nu^2 - 1}} (\eta_{\mu\nu} dx^\mu dx^\nu + dz^2). \quad (2.11)$$

In these coordinates, the \mathcal{M}_ν^- and \mathcal{M}_ν^+ regions defined in (2.9) are given by

$$\begin{aligned} \mathcal{M}_\nu^+ &= \mathcal{M}_\nu|_{z \in (0, z_b]}, & \mathcal{M}_\nu^- &= \mathcal{M}_\nu|_{z \in [z_b, \infty)} & \text{if } \nu < 1, \\ \mathcal{M}_\nu^- &= \mathcal{M}_\nu|_{z \in (0, z_b]}, & \mathcal{M}_\nu^+ &= \mathcal{M}_\nu|_{z \in [z_b, \infty)} & \text{if } \nu > 1, \end{aligned} \quad (2.12)$$

where

$$z_b = \frac{L}{\eta r_b} \frac{1}{|\nu^2 - 1|}. \quad (2.13)$$

The special case $\nu = 1$ is the linear dilaton spacetime, for which

$$z = \pm \frac{L}{r_b \eta} \log \frac{r}{L}. \quad (2.14)$$

Importantly, the domain in this case is $z \in \mathbb{R}$. The freedom of sign in (2.14) is reminiscent of the conformal inversion symmetry of the LD spacetime [27].

2.4 The Black Hole

Extending the result from [82], the \mathcal{M}_ν^- spacetime admits a planar black hole solution:⁵

$$ds_{\nu, r_b}^2 = \left(\frac{r}{L}\right)^2 (-f(r)d\tau^2 + dx^2) + \frac{1}{f(r)} \left(\frac{r}{r_b}\right)^{2\nu^2} \frac{1}{(\eta r)^2} dr^2, \quad (2.15)$$

with the blackening factor

$$f(r) = 1 - \left(\frac{r_h}{r}\right)^{D-1-\nu^2}, \quad (2.16)$$

where r_h is the location of the horizon.

2.5 On Singularities and Boundaries

For clarity, throughout this work, we refer to a boundary as a *regular* boundary, to emphasize the distinction with the notion of conformal boundary. In the vicinity of a regular boundary, spacetime is isomorphic to the half flat space. A conformal boundary is similarly defined, but up to a suitable Weyl rescaling to flat space.

2.5.1 Metric Zeros and Singularities

We show a condition under which the vanishing of the whole metric implies divergence of the curvature.

We go to conformal coordinates denoted (x^μ, z) for which the coefficients of the general metric (2.2) are $g_{xx}(z) = g_{zz}(z) \equiv a(z)$. We refer to a zero of the warp factor $a(z)$ as a *metric zero*. The curvature scalar in conformal coordinates is

$$R = -(D-1) \frac{(D-6)(a')^2 + 4aa''}{4a^3}, \quad (2.17)$$

where the prime ($'$) denotes derivative with respect to z .

⁵The black hole in the 4D linear dilaton case was independently found in [99].

We assume that the scale factor $a(z)$ goes to zero at a *finite* value z_s . Assuming that z_s is approached from above, we have $\lim_{z \rightarrow z_s^+} \frac{1}{a(z)} = \infty$. We then use the following property:

$$\text{If } a(z) \text{ vanishes at finite } z_s, \text{ then: } \lim_{z \rightarrow z_s^+} \frac{a'(z)}{a(z)} = \infty. \quad (2.18)$$

This property is shown in App. A using the mean value theorem — with the mild assumption that $\frac{a'(z)}{a(z)}$ is strictly monotonic in the vicinity of the singularity. Using the definition of the curvature (2.17), (2.18) implies that $\lim_{z \rightarrow z_s^+} R(z) = \infty$. That is, the scalar curvature diverges at z_s . Summarizing:

$$\text{If there is a conformal coordinate } z_s < \infty \text{ for which the scale factor satisfies } a(z_s) = 0, \text{ then there is a curvature singularity at } z_s. \quad (2.19)$$

We emphasize that the assumption of *finite* z_s is key for the proof. If $z_s = \infty$, the mean value theorem does not apply, and thus Prop. (2.18) does not hold. As an example of non-applicability, AdS space in conformal coordinates $a(z) \propto z^{-2}$, for which $z_s = \infty$, has $a(z_s) = 0$, yet it has finite R at z_s since R is constant everywhere.

Finally, when a singularity appears, the general relativity description breaks down and we must cut off spacetime. In our case we have to require that $z > z_s$, which is a regular boundary. In other words, the metric zero describes a singularity that truncates spacetime.

2.5.2 The \mathcal{M}_ν spacetime case

We summarize the structure of boundaries and singularities of the \mathcal{M}_ν spacetime, bearing in mind the general discussion of Sec. 2.5.1.

In \mathcal{M}_ν , the scalar curvature diverges at $r \rightarrow 0$ for any $\nu > 0$. There is thus a curvature singularity at $r = 0$, which lies in the \mathcal{M}_ν^- part of the spacetime. The singularity is labeled as “good” in the sense of Refs. [44, 100] if $\nu < \sqrt{d}$. This is confirmed by [82] for $d = 4$ where it is found that $\nu \in [0, 2)$ is the range of values for which the singularity can get censored by a black hole horizon. Regarding the \mathcal{M}_ν^+ spacetime, it does not feature any singularity for any ν .

We now go to conformal coordinates to analyze boundaries, for which $a(z) \propto z^{\frac{2}{\nu^2-1}}$, see [82] for details. For $\nu < 1$ there is a conformal timelike boundary, however it belongs to \mathcal{M}_ν^+ . For $\nu > 1$ there is a regular boundary at $z = 0$. In the special case of $\nu = 1$ (linear dilaton) the boundaries are null, the Penrose diagram is the same as Minkowski’s, and the singularity is at a spatial infinity of the causal diamond.

We can see that Prop. (2.19) applies. For $\nu > 1$, we have $a(z_s) = 0$ at a finite conformal distance $z_s = 0$. Using (2.19) we conclude that there is a curvature singularity there, that coincides with the regular boundary. That is, the singularity cuts off space to $z > 0$. For $\nu \leq 1$, we have instead $z_s = \infty$. In that case Prop. (2.19) does not apply: there is a singularity for $\nu > 0$ but not when $\nu = 0$ (AdS case).

3 Holographic Confinement

We classify the \mathcal{M}_ν^- dilaton gravity backgrounds in terms of confinement. In the holographic view of confinement, a Wilson loop on the boundary is evaluated as a string extending into the bulk⁶. The background is said to be *confining* if the Wilson loop features an area law, i.e. if the corresponding $q\bar{q}$ potential grows linearly with $q\bar{q}$ separation. In the \mathcal{M}_ν^- dilaton gravity background considered here, the string is attached to the brane located at $r = r_b$.

3.1 The Holographic Wilson Loop

We review the holographic computation of the quark-antiquark potential, here generalized to any bulk dimension. The potential energy $V(\ell)$ of a static $q\bar{q}$ pair separated by a distance ℓ is conjectured to be computed in the bulk by

$$TV(\ell) \equiv S_{\text{NG}}[x_{\text{cl}}^M(\sigma, \tau)]. \quad (3.1)$$

S_{NG} is the Nambu-Goto action, $x^M(\sigma, \tau)$ is the worldsheet embedding for the string attached to a rectangle of size (T, ℓ) on the brane, and $x_{\text{cl}}^M(\sigma, \tau)$ describes the string configuration of minimal surface, that we refer to as the classical configuration. The Nambu-Goto action in (3.1) is “on-shell” in the sense that it is evaluated on the classical configuration.

We have

$$S_{\text{NG}}[x^M(\sigma, \tau)] = T_f \int d\tau d\sigma \sqrt{\det(-\hat{g}_s)} \quad (3.2)$$

where \hat{g}_s denotes the induced metric on the worldsheet, and T_f is the string tension. The worldsheet embedding $x^M(\sigma, \tau)$ defines the D -dimensional string frame metric $(g_s)_{MN}$ as

$$(\hat{g}_s)_{\alpha\beta} = (g_s)_{MN} \partial_\alpha x^M \partial_\beta x^N. \quad (3.3)$$

Assuming that the string frame metric takes the diagonal form

$$ds_s^2 = -g_{s,00} dt^2 + g_{s,rr} dr^2 + g_{s,ii} dx_i^2, \quad (3.4)$$

choosing worldsheet coordinates $\tau = t$, $\sigma = x^1 \equiv x$, and assuming invariance in time, one obtains [101]

$$S_{\text{NG}}[x^M(\sigma, \tau)] = T_f \int dx \sqrt{h^2(r) + k^2(r)r'^2}, \quad (3.5)$$

with

$$h^2(r) = g_{s,00}(r)g_{s,ii}(r), \quad k^2(r) = g_{s,00}(r)g_{s,rr}(r), \quad (3.6)$$

and $r' \equiv \frac{dr}{dx}$. The classical solution, i.e. the configuration of minimal length, is denoted by $r_{\text{cl}}(x)$.

⁶See e.g. [48–53, 101] for seminal papers and [9] for a detailed study in holographic QCD. Here we mostly use [9, 101].

Assuming no restriction on the domain of coordinates, the string geodesic equation that determines $r_{\text{cl}}(x)$ can be readily deduced from Eq. (3.5),

$$\frac{dr}{dx} = \pm \frac{h(r)}{k(r)} \frac{\sqrt{h^2(r) - h_0^2}}{h_0}, \quad (3.7)$$

with $h_0 = h(r_0)$, where r_0 corresponds to the tip of the geodesic which satisfies $\left. \frac{dr}{dx} \right|_{r_0} = 0$. h_0 can be considered as a constant of motion that parameterizes the geodesics.

Finally, for a given spacetime background, the string frame metric $(g_s)_{MN}$ is obtained by converting frames in the low-energy effective action. The string and Einstein frames are related in any dimension by use of the conformal rescaling

$$g_{MN} = e^{-2\bar{\phi}} g_{s,MN}, \quad (3.8)$$

where $\bar{\phi} = \frac{\phi}{\sqrt{(D-2)M_D^{D-2}}}$ is the reduced dilaton field introduced in section 2. Starting from the Einstein frame action (2.1), we find the bulk action in string frame

$$\mathcal{S}_s = \frac{M_D^{D-2}}{2} \int d^D x \sqrt{g_s} e^{-(D-2)\bar{\phi}} \left({}^{(D)}R_s + (D-2)^2 (\partial_M \bar{\phi})^2 - \bar{V}_s(\bar{\phi}) \right), \quad (3.9)$$

where $\bar{V}_s = 2(D-2)e^{-2\bar{\phi}}\bar{V}$. The low-energy string effective action in the usual convention from e.g. [102–104] is recovered by normalizing the dilaton field as $\bar{\phi}_s \equiv \frac{D-2}{2}\bar{\phi}$.

3.2 String Shape in Dilatonic Background

We apply the above formalism to our dilatonic background \mathcal{M}_ν with Einstein metric (2.7). The string frame metric and derived quantities are


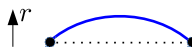
$$ds_{\nu, r_b, s}^2 = e^{2\bar{\phi}_b} \left(\frac{r_b}{L} \right)^2 \left(\frac{r}{r_b} \right)^{2-2\nu} \eta_{\mu\nu} dx^\mu dx^\nu + e^{2\bar{\phi}_b} \frac{1}{\eta^2 r_b^2} \left(\frac{r}{r_b} \right)^{2\nu^2 - 2\nu - 2} dr^2, \quad (3.10)$$

$$h(r) = e^{2\bar{\phi}_b} \left(\frac{r_b}{L} \right)^2 \left(\frac{r}{r_b} \right)^{2-2\nu}, \quad k(r) = e^{2\bar{\phi}_b} \frac{1}{\eta L} \left(\frac{r}{r_b} \right)^{\nu^2 - 2\nu}. \quad (3.11)$$

We can notice that the metric is Minkowski when $\nu = 1$: the linear dilaton background is flat in the string frame. The reduced potential is $\bar{V}_s = -(D-2)(D-1-\nu^2)k^2 e^{2(\nu-1)\bar{\phi}}$. In the linear dilaton case, \bar{V}_s reduces to a constant, which is consistent with results in the literature. The value is $\bar{V}_s|_{\nu=1} = -(D-2)^2 k^2$.

To understand the behavior of the string in our dilatonic background, let us consider a static string configuration with endpoints lying at coordinates $(0, \tilde{r})$ and $(\Delta x, \tilde{r})$ in the bulk. In the critical case $\nu = 1$ i.e. the linear dilaton, the classical string configuration simply is the straight line, $r_{\text{cl}}(x) \equiv \tilde{r}$. We establish a useful qualitative property:

If $\nu < 1$ (resp. $\nu > 1$) the classical string configuration bends towards $r < \tilde{r}$ (resp. $r > \tilde{r}$). (3.12)

Schematically,  for $\nu < 1$ and  for $\nu > 1$.

We show this at the infinitesimal level as follows. We consider the straight line configuration, given by $r(x) \equiv \tilde{r}$ for all x . The corresponding Nambu-Goto action is $\tilde{\mathcal{S}}_{\text{NG}} = T_f \Delta x h(\tilde{r})$. We then consider a small perturbation to the straight line, $r(x) = \tilde{r} + \delta r(x)$, with $\delta r \ll \tilde{r}$ for all x . The action for this perturbed configuration is

$$\mathcal{S}_{\text{NG}} = \tilde{\mathcal{S}}_{\text{NG}} + \delta \mathcal{S}_{\text{NG}}, \quad \delta \mathcal{S}_{\text{NG}} = T_f \int dx (h'(\tilde{r}) \delta r(x) + O(\delta r^2)), \quad (3.13)$$

with $h'(r) = \frac{dh(r)}{dr}$. Let us further assume that the perturbation is towards $r > \tilde{r}$, i.e. $\delta r(x) > 0$ for all x . It follows that

$$\text{sign}(\delta \mathcal{S}_{\text{NG}}) = \text{sign}(h'(\tilde{r})). \quad (3.14)$$

This relation implies that, relative to the straight line configuration, the perturbed configuration has lower (higher) energy if $h'(\tilde{r}) < 0$ ($h'(\tilde{r}) > 0$). Similarly, for $\delta r(x) < 0$ (in which case the perturbation is toward $r < \tilde{r}$) the perturbed configuration has lower energy if $h'(\tilde{r}) > 0$.

Using the explicit expression of h in Eq. (3.11), it follows that, at the infinitesimal level, string configurations with $r < \tilde{r}$ (resp. $r > \tilde{r}$) are favored if $\nu < 1$ (resp. $\nu > 1$). This proves the infinitesimal version of Prop. (3.12).⁷

We can also derive Prop. (3.12) at the finite level by inspecting the classical string configurations. Assuming that the tip of the classical configuration r_0 is inside the spacetime, the classical configuration is determined by the geodesic equation (3.7). We see from this equation that h_0 must be smaller than $h(r_{\text{cl}})$ for all values of r_{cl} . This condition is satisfied in the $r_0 < r_{\text{cl}} < \tilde{r}$ region if h is monotonic increasing, and conversely in the $r_0 > r_{\text{cl}} > \tilde{r}$ region if h is monotonic decreasing. Since h increases if $\nu < 1$, and decreases if $\nu > 1$, we obtain again Prop. (3.12).

Finally, we notice that the scalar curvature in string frame is

$$R_s = -(D-1)(\nu-1)^2(D+2\nu)e^{-2\bar{v}_b} \eta^2 \left(\frac{r}{r_b}\right)^{2\nu(1-\nu)}. \quad (3.15)$$

Hence the curvature singularity in string frame is at $r \rightarrow \infty$ for $\nu < 1$ and $r = 0$ for $\nu > 1$. Hence qualitatively we can say that, the string living in the \mathcal{M}_ν background is *repelled* by the (string frame) singularity. Accordingly, for $\nu = 1$ we have $R_s = 0$, hence there is no singularity, therefore the string is straight.

⁷One may consider the most general configuration for which $\delta r(x) > 0$ on some (possibly disjoint) subdomain I_+ of $(0, \Delta x)$ and $\delta r(x) < 0$ on its complement I_- . In this case the analysis can be applied piecewise to each subdomain where $\delta r(x)$ has definite sign. Assuming for example $\nu > 1$, we know that this configuration has higher energy than a configuration that is identical on I_+ and has $\delta r(x) > 0$ on I_- i.e. that has $\delta r(x) > 0$ everywhere. This is true for any configuration, hence the configuration of lower energy necessarily has $\delta r(x)$ of definite sign over the whole $(0, \Delta x)$ interval. It is thus sufficient to focus on this case.

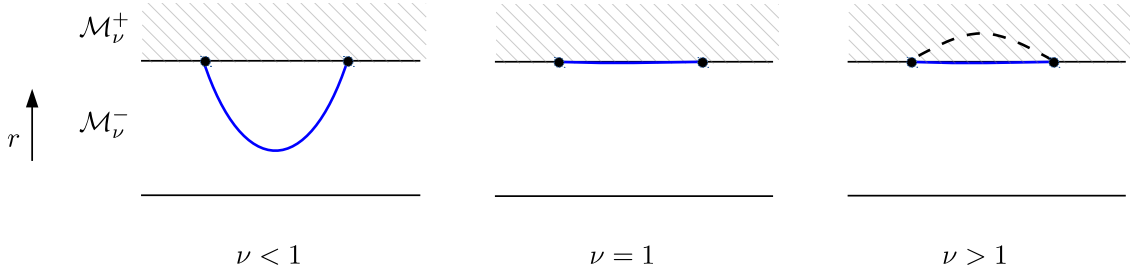


Figure 2. The classical string attached to the brane in the \mathcal{M}_ν^- background. The configuration is a straight line for both $\nu = 1$ (because it is geodesic) and $\nu > 1$ (because it is stuck to the brane). In both cases the background is confining with same string tension $T_s = T_f e^{2\bar{\phi}_b} \left(\frac{r_b}{L}\right)^2$.

3.3 Confinement

We consider the \mathcal{M}_ν^- spacetime, for which $0 < r < r_b$. The string is anchored to the brane at $r = r_b$. The behavior of the classical configuration is obtained using Prop. (3.12).

If $\nu < 1$, the classical string configuration bends towards $r < r_b$. In that case the geodesic equation (3.7) applies. The string length is given by [101]

$$\ell = \int_{\text{cl}} dx = 2 \int_{r_0}^{r_b} dr \frac{k(r)}{h(r)} \frac{h_0}{\sqrt{h^2(r) - h_0^2}}, \quad (3.16)$$

and the potential is given by

$$V(\ell) = T_f \int_{\text{cl}} \mathcal{L} dx = 2T_f \int_{r_0}^{r_b} dr \frac{k(r)}{h(r)} \frac{h^2(r)}{\sqrt{h^2(r) - h_0^2}}. \quad (3.17)$$

The integrals can be done analytically, but the expressions are not particularly enlightening. We find numerically that $V(\ell)$ is not linearly proportional to ℓ for any value of r_0 , except in the $\nu \rightarrow 1$ limit.

If $\nu = 1$, the classical string follows a straight geodesic along $r = r_b$. We find

$$V(\ell) = T_f e^{2\bar{\phi}_b} \left(\frac{r_b}{L}\right)^2 \ell. \quad (3.18)$$

That is, the potential grows linearly with ℓ , for any ℓ . The linear dilaton is therefore a confining background with string tension

$$T_s = T_f e^{2\bar{\phi}_b} \left(\frac{r_b}{L}\right)^2. \quad (3.19)$$

The same result is obtained when taking the $\nu \rightarrow 1$ limit from (3.16) and (3.17).⁸

If $\nu > 1$, the string would bend towards $r > r_b$, however this region does not exist in \mathcal{M}_ν^- . Using (3.12), the allowed configuration of lower energy is the straight line along $r = r_b$. We find again the confining potential Eq. (3.18) because $h(r_b)$ is independent on ν ,

⁸A related analysis of confinement from the viewpoint of string theory can be found in [105].

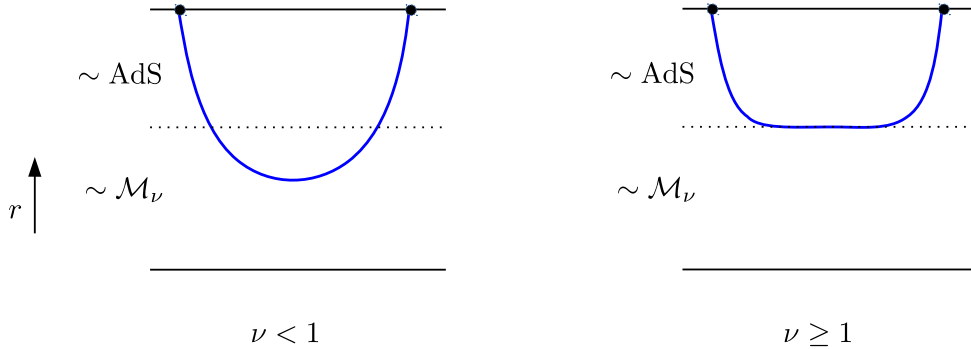


Figure 3. *The classical string attached to a brane in an asymptotic AdS background. For $\nu \geq 1$ the string enters the asymptotic \mathcal{M}_ν region only up to a finite value of r . Accordingly it asymptotically follows an area law with tension $T_s = T_s e^{2\bar{\phi}_b} \left(\frac{r_b}{L}\right)^2$.*

hence $h(r_b)|_{\nu>1} = h(r_b)|_{\nu=1}$. The string tension is again given by Eq. (3.19). These features are summarized in Fig. 2.

In terms of the curvature singularity in string frame, we can say that confinement occurs if the singularity is in \mathcal{M}_ν^- , such as the string is repelled as shown in the $\nu > 1$ case of Fig. 2, or if it is absent such that the string remains straight as in the $\nu = 1$ case of Fig. 2.

3.4 Comparison to Asymptotically AdS backgrounds

The remarkably simple picture of confinement obtained here is consistent with the one derived in [9]. Ref. [9] considers a class of 5D dilatonic spacetimes which is asymptotically AdS in the UV and analogous to the \mathcal{M}_ν background in the IR. In our coordinates the AdS region is at large r , hence the IR region is similar to the \mathcal{M}_ν^- background considered here. Roughly speaking, spacetime continues into asymptotic AdS instead of stopping at the brane. The behavior of the string in the asymptotically AdS backgrounds can be easily understood using Prop. (3.12).

Let us consider a string anchored to a brane in the AdS region, i.e. at large r , with endpoints separation Δx in Minkowski distance.⁹ For small Δx , the string only knows about the AdS background and thus bends towards smaller r , as dictated by Prop. (3.12) with $\nu = 0$. Increasing Δx , the tip of the string enters in the non-AdS IR region. In this regime, if $\nu < 1$, the string keeps entering further into the IR since it still tends to bend towards smaller r . But if, instead, $\nu > 1$, the part of the string in the IR wants to bend towards large r as dictated by (3.12). That is, for $\nu > 1$ the tendencies in the UV and IR regions are opposite. As a result the string does not go beyond a certain point in the IR. These behaviors are sketched in Fig. 3.

This phenomenon of saturation matches the behavior reported in [9], which was identified in terms of a non-monotonicity in the scale factor. It turns out that this saturation

⁹Since the asymptotic AdS spaces considered here are cutoff by the brane, the string self-energy [106–108] is regularized it does not feature UV divergences.

implies confinement asymptotically. The confining behavior is easily understood from the viewpoint of our analysis, for example by replacing the shaded region in Fig. 2 by asymptotic AdS. At large Δx , for $\nu \geq 1$ the main contribution to the string length would be the straight segment, that implies confinement as shown in section 3.3.

4 Holographic Entanglement Entropy

In a given quantum system, the entanglement of a given subsystem with the rest of the system can be quantified using the entropy. This entanglement (or von-Neumann) entropy (EE) is defined via tracing out the states outside the subsystem. It can be viewed as the amount of entropy for an observer that only receives information from the subsystem. Entanglement entropy is typically used as a tool to understand quantum systems.

The entanglement entropy in holographic theories admits a simple geometric description [109–118]. The interplay of holographic entanglement entropy (HEE) with confinement has been explored in [65–76]. Here our goal is to understand HEE in the simple setup of dilaton gravity. We explore the HEE described by the \mathcal{M}_ν^- background, and also establish some properties of HEE for more general warped metrics.

The subsystem of our interest is supported on a region A of the brane. Focusing on a spacelike region, the HEE is given by the Ryu-Takayanagi (RT) formula [109]

$$S_A = \frac{\text{Area}(\gamma_A)}{4G_N}, \quad (4.1)$$

where γ_A is the surface of minimal area anchored to the boundary of A .¹⁰ The area of γ_A is computed using the Einstein frame metric.

In this work we choose the simplest region for A : a $(d-1)$ -dimensional strip with width L_A at a given time $t=0$.

In the following we first establish some properties for the general warped metric defined in (2.2), before turning to the detailed analysis of the \mathcal{M}_ν^- background.

4.1 Elementary Properties

We can identify two possible surfaces: *i*) a smooth surface generated by the shift of a curve with base $\Delta x = L_A$, and *ii*) a squared-shape surface that extends from the brane ($r = r_b$) down to $r = 0$. The surfaces are respectively denoted γ_U and γ_\perp and are depicted in Fig. 4.

We are interested in the behavior of S_A as a function of the strip width L_A . Anticipating the HEE results, the existence of these two surfaces is the cause of *phase transitions* in the EE, which happen because either γ_U or γ_\perp have minimal area depending on the subsystem size.

The surfaces in Fig. 4 are parametrized by an embedding $x^M = F(\sigma^m)$ where σ^m are the d coordinates for the points belonging to the surface. We choose $F(\sigma^m) = (\sigma^m, u(\sigma^1))$,

¹⁰The RT formula should generally be accompanied by a homology condition that dictates how the minimal surface behaves with respect to black holes (see [119–121]). In this section we do not consider black holes, hence the bulk has trivial homology and no additional conditions need to be specified.

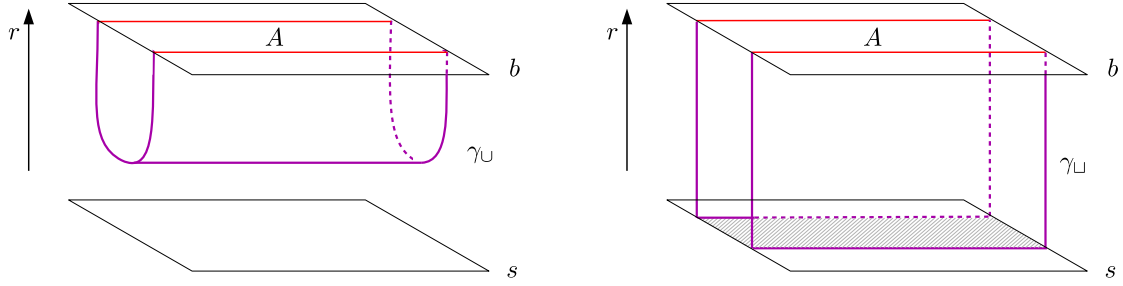


Figure 4. The candidate minimal surfaces anchored to the surface of a $(d-1)$ -strip at a given time on the brane. Left: The smooth surface. Right: The square surface.

such that the σ^m are identified with (r, x^1, \dots, x^{d-2}) . In Fig. 4, x^{d-1} is the direction which crosses the strip. The profile of the minimal surface is given by $x^{d-1} = u(r)$. The vertical sides of the square surface correspond to $x^{d-1} = \text{cst}$. The longitudinal directions collectively represent the other (x^1, \dots, x^{d-2}) directions. Working in the Einstein frame with the general metric (2.2), the induced metric for the surface is then

$$ds_{\text{ind}}^2 = \left(g_{rr}(r) + u'^2(r)g_{xx}(r) \right) dr^2 + g_{xx}(r) \left((dx^1)^2 + \dots + (dx^{d-2})^2 \right). \quad (4.2)$$

4.1.1 Smooth Surface

From the induced metric (4.2), we can compute the spatial area of the smooth surface as

$$\text{Area}(\gamma_U) = 2A_{d-2} \int_{r_0}^{r_b} dr a(r)^{\frac{d-1}{2}} \sqrt{b^2(r) + u'^2(r)}, \quad (4.3)$$

with $a(r) = g_{xx}(r)$, $b(r) = \sqrt{\frac{g_{rr}(r)}{g_{xx}(r)}}$ and $A_{d-2} = \int dx^1 \dots dx^{d-2}$.

The surface is minimal when the $u(r)$ function satisfies the Euler-Lagrange equation

$$\frac{du(r)}{dr} = U \frac{b(r)}{\sqrt{a(r)^{d-1} - U^2}}. \quad (4.4)$$

Here U is a constant that characterizes the curve $x^{d-1} = u(r)$. Since $\frac{dr}{du}$ vanishes if $a^{d-1}(r) = U^2$, the U constant is identified as $U \equiv a^{\frac{d-1}{2}}(r_0)$ where r_0 is the coordinate of the ‘‘tip’’ of the curve. The strip width L_A and the tip of the curve r_0 are tied due to the solutions of (4.4), i.e. we have $L_A = L_A(r_0)$.

4.1.2 Square Surface and Singularity

The area of the square surface is the one of the vertical piece plus the one of the strip at $r = 0$. The existence of γ_{\square} requires that the vertical piece exist in a first place. In terms of the general warped metric (2.2), this is true if there is a value of r_0 such that the metric coefficient $a(r)$ satisfies $a(r_0) \equiv 0$. The bottom part of the square surface is localized at r_0 ,

which implies that its area is vanishing due to the vanishing of the scale factor. Hence we have always that

$$\text{Area}(\gamma_{\sqcup}) = 2A_{d-2} \int_0^{r_b} dr a(r)^{\frac{d-1}{2}} b(r), \quad (4.5)$$

for *any* L_A , i.e. the area of the square surface does not depend on the strip width.

Assuming conformal coordinates (x^μ, z) in the general metric such that $b(z) = 1$ for all z , the existence of γ_{\sqcup} requires $a(z_0) \equiv 0$, which implies that z_0 is a metric zero. Applying Prop. (2.19), this implies the existence of a curvature singularity at $z = 0$, on which the square surface ends.

4.1.3 A Necessary Condition for HEE phase transition

The area for the square surface may be finite or infinite, depending on the behavior of the integral $\int_0^{r_b} dr a(r)^{\frac{d-1}{2}} b(r)$. If the integral diverges, the γ_{\sqcup} has infinite area and thus the minimal area is the one of γ_U . In that case, no phase transition can happen in the HEE. Therefore,

$$\begin{aligned} &\text{A HEE phase transition can occur only if} \\ &\text{the integral } \int_0^{r_b} dr a(r)^{\frac{d-1}{2}} b(r) \text{ is finite.} \end{aligned} \quad (4.6)$$

This is a necessary condition. This condition is automatically satisfied if there is a metric zero at finite conformal distance. Thus the possibility of a HEE phase transition is related via Prop. (2.19) to the existence of a singularity at finite conformal distance.

4.1.4 The Near-Brane Surface

When r_0 is close to r_b , the smooth surface stays near the brane. In that limit the equations (4.3) and (4.4) are dominated by the square root term $(a(r)^{d-1} - a(r_0)^{d-1})^{-1/2}$, while the other factors can be taken at $r \sim r_b$. This implies that

$$\text{Area}(\gamma_{\sqcup}) \stackrel{r_0 \sim r_b}{\approx} A_{d-2} L_A a(r_b)^{\frac{d-1}{2}}. \quad (4.7)$$

That is, the area of γ_{\sqcup} tends to the area of the basis region, $\text{Area}(\gamma_{\sqcup}) \approx \text{Area}(A)$. The (4.7) limit can also be understood as the area for “small” γ_U , since the approximation is valid in the small L_A limit.

4.2 Phase Transition and Boundaries

This section establishes some properties of the HEE for the general warped metric of (2.2). All the properties obtained here appear explicitly in the case of the \mathcal{M}_V^- background presented in section 4.4, see in particular Fig. 6.

A necessary condition for a phase transition of HEE to occur is that the width of the base of the γ_{\sqcup} surface be bounded from above, i.e. $L_A < L_A^{\max}$ with $L_A^{\max} < \infty$. In such a situation, whenever one considers a strip A with $L_A > L_A^{\max}$, only the γ_U remains available, hence γ_U is automatically the minimal surface. Here we establish a relation between the

boundedness of the base of γ_U , i.e. the existence of a finite L_A^{\max} , and the existence of a singularity at finite conformal distance.

As seen in section 2.5, the spacetime background may feature either a regular or a conformal timelike boundary along constant r slices. Since this distinction is done using conformal coordinates, here we go to conformal coordinates (x^μ, z) , that imply $b(z) = 1$ for any z such that the warped metric (2.2) is manifestly conformally flat. We assume in this subsection that the metric coefficients are *strictly monotonic*.¹¹

Using the Euler-Lagrange equation (4.4), we know that the width of the base of γ_U satisfies

$$L_A(z_0) = U \int_{z_0}^{z_b} \frac{dz}{\sqrt{c(z) - U^2}}, \quad (4.8)$$

where $c(z) = a(z)^{d-1}$ and $U^2 = c(z_0)$, with z_0 the coordinate of the tip of the curve. If $c(z)$ is monotonically increasing (resp. decreasing) we have $z_0 < z_b$, (resp. $z_0 > z_b$), such that $c(z) > c(z_0)$ under the integral in all cases. In the following we choose c to be increasing and thus $z_0 < z_b$.

We denote the domain of $a(z)$ by $[z_*, z_b]$. The lower bound z_* may be either finite or infinite. We assume in this subsection that U can reach 0, which is required for the square surface to exist (see section 4.1.2). Since $U^2 = c(z)$ with c monotonic, this condition corresponds necessarily to having $c(z_*) = 0$. Using Prop. (2.19), if z_* is finite then there is a curvature singularity at $z_* \equiv z_s$. If z_* is infinite, no statement can be made and z_* can be simply thought of as the boundary for z .

4.2.1 Sufficient Conditions for HEE Phase Transition

We rewrite the integral in (4.8) as

$$\int_{U^2}^{y_b} \frac{dy}{c'[c^{-1}(y)]\sqrt{y - U^2}}, \quad (4.9)$$

where we used the change of variable $c(z) \equiv y$, with $y_b \equiv c(z_b)$, $y_0 \equiv c(z_0) = U^2$. The function c^{-1} is the inverse of the c function and $c'[x]$ is the derivative of c with respect to its argument x .

Since by assumption the c function is monotonic on the open interval (z_*, z_b) , there exists $B > 0$ such that $c'(z) > B$ for all $z \in (z_*, z_b)$. Hence the inverse $1/c'(z)$ is defined on (z_*, z_b) . However it is not guaranteed that $1/c'(z)$ is defined at the endpoints, where it might blow up, e.g. $1/c'(z_*) = \infty$. In such a case the integral (4.9) is improper.

A sufficient condition for the integral (4.9) to be finite is if the lower bound z_* is finite and $1/c'(z)$ is defined on the *closed* interval $[z_*, z_b]$. In that case, having a continuous function on a closed interval, the boundedness theorem implies that there exists an upper bound \bar{B} on $1/|c'(z)|$ on $[z_*, z_b]$. As a result the integral (4.9) is bounded from above by $\bar{B} \int_{U^2}^{y_b} dy (y - U^2)^{-1/2} = 2\bar{B}\sqrt{y_b - U^2}$. The comparison theorem for integrals then implies that (4.9) is bounded from above for any U . Going back to the definition (4.8) we use that U

¹¹The results of this subsection can be extended with little effort to metrics that are monotonic in a finite region near the singularity.

is bounded from above since $c(z_0) < c(z_b)$ for all $z_0 < z_b$ because c is monotonic increasing. It follows that $L_A(z_0)$ is bounded from above for any z_0 , i.e. there exists $L_A^{\max} < \infty$. The same conclusion happens if one chooses the convention that c is decreasing and $z_0 > z_b$. Putting the pieces together, we conclude that

If the function $1/c'(z)$ is defined on the *closed* interval $[z_*, z_b]$ with finite z_* , then the holographic entanglement entropy exhibits a phase transition. (4.10)

Since having a metric zero at finite z_* implies a curvature singularity by Prop. (2.19), the condition in (4.10) requires $1/c'(z)$ to be defined on the singularity $z_* \equiv z_s$.

We emphasize that (4.10) is only a sufficient condition for the existence of HEE phase transition. For example, when applied to the \mathcal{M}_ν^- metric, for which $c(z) \propto z^{\frac{2(d-1)}{\nu^2-1}}$ and a regular boundary $z_s = 0$ exists for $\nu > 1$, we have $1/c'(z) \propto z^{\frac{2d-1-\nu^2}{1-\nu^2}}$. This is finite at $z \rightarrow z_s$ only for $\nu > \sqrt{2d-1}$. This condition does not ensure the existence of the HEE phase transition in the \mathcal{M}_ν^- background for any d , since the absence of bad singularity requires that $\nu < \sqrt{d}$ (see section 2.5).

We find a slightly better sufficient condition by bounding $dc^{-1}(y)/dy \equiv [c^{-1}]'(y) = 1/c'[c^{-1}(y)]$ with the U -dependent upper bound $[c^{-1}]'(U^2)$. Such a bound is set up to include the situation where $[c^{-1}]'(y)$ blows up at $y \rightarrow 0$, that is not taken into account by the sufficient condition (4.10). We put this upper bound in the definition (4.8) and require finiteness for any U . We obtain that L_A is bounded from above for any U (i.e. any z_0) if the condition

$$U \times [c^{-1}]'(U^2) < \infty \quad (4.11)$$

is satisfied for all U . Using $U^2 = c(z_0)$ and $c(z) = a(z)^{d-1}$, we obtain the final condition that is summarized as

If the function $\frac{a^{\frac{3-d}{2}}(z_0)}{a'(z_0)}$ is bounded from above for all $z_0 \in (z_*, z_b]$, then the HEE exhibits a phase transition. (4.12)

When applied to the \mathcal{M}_ν^- metric, the criterion from (4.12), is $\nu > \sqrt{d}$. While it is better than property (4.10), the value lies right at the consistency limit for bad singularities, hence the sufficient condition (4.12) does not ensure the existence of the HEE phase transition in the \mathcal{M}_ν^- background for any d .

4.2.2 Pairs of Smooth Surfaces

In the presence of the singularity at finite conformal distance, the fact that $L_A(z_0)$ tends to zero when $z_0 \rightarrow z_s$ implies that there exist *two* smooth surfaces γ_U , that both solve the Euler-Lagrange equation, for a given $L_A < L_A^{\max}$. This is because, for a given L_A , in addition to the large surface with $z_0 \sim z_s$, there is always a small surface closer to the brane, whose area is given by (4.7). By continuity of L_A in z_0 , for any $L_A < L_A^{\max}$ there must exist two smooth surfaces with different z_0 .

In summary, the presence of a singularity at finite conformal distance implies the existence of a pair of smooth surfaces.

4.3 Smooth Surfaces in the \mathcal{M}_ν^- background

In the \mathcal{M}_ν^- background we can actually compute the smooth surfaces. Using the Einstein frame metric (2.7), the a, b functions are

$$a(r) = \frac{r^2}{L^2}, \quad b(r) = \frac{r^{\nu^2-2} L}{r_b^{\nu^2} \eta}. \quad (4.13)$$

The general solution to the Euler-Lagrange equation (4.4) is

$$u = \frac{iL^2 U}{\eta(1-\bar{\nu}^2)(d-1)} \frac{r^{\nu^2-1}}{r_0^{d-1} r_b^{\nu^2}} {}_2F_1 \left(\frac{1}{2}, \frac{1}{2}(\bar{\nu}^2-1); \frac{1}{2}(\bar{\nu}^2+1); \frac{r^{2(d-1)}}{r_0^{2(d-1)}} \right) + \text{cst}, \quad (4.14)$$

where

$$\bar{\nu}^2 = 1 + \frac{\nu^2-1}{d-1}, \quad (4.15)$$

for $\nu \neq 1$ and $r_0 \neq 0$. We show in App. B how to compute the general case with arbitrary d from the $d=2$ case using the matching given in (4.15).

The $\nu=1$ (LD) case gives

$$u = \frac{UL^2}{\eta r_b r_0^{d-1} (d-1)} \arctan \left(\sqrt{\frac{r^{2(d-1)}}{r_0^{2(d-1)}} - 1} \right) + \text{cst} \quad (4.16)$$

for any d .

Tip

The approximation for r_0 in the $r_0 \ll r_b$ limit is

$$\frac{r_b}{r_0} \sim \left(\frac{\eta L_A r_b}{L} \right)^{\frac{1}{1-\nu^2}}. \quad (4.17)$$

The combination $\frac{\eta L_A r_b}{L}$ will naturally appear in the asymptotic and critical behaviors obtained throughout the rest of the section.

Shape

The smooth surfaces have qualitatively different behaviors in the $\nu < 1$, $\nu = 1$ and $\nu > 1$ cases.

- For $\nu < 1$, the strip width L_A increases indefinitely when r_0 approaches 0, i.e. we have $L_A \in [0, \infty)$.
- In contrast, when $\nu = 1$ the width reaches a saturation, i.e. L_A is bounded from above with $L_A \in [0, \frac{\pi L}{(d-1)\eta r_b}]$ (see Eq. (4.19) below).

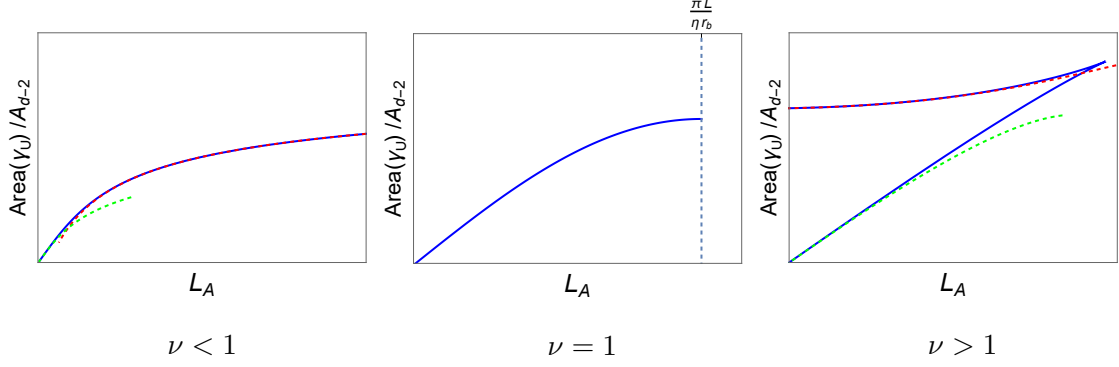


Figure 5. Area of the smooth surface γ_U as a function of the strip width L_A . Plain lines are exact results for $\nu = 0.5, 1$ and 1.5 . Red and green dashed lines are respectively approximations for $r_0 \ll r_b$ (4.18) and for $r_0 \approx r_b$ (4.7).

- Finally, for $\nu > 1$, starting from $r_0 \sim r_b$, the base of the smooth surface increases, reaches a maximum and then decreases to zero when r_0 approaches 0. Thus for $\nu > 1$ there exist *two* smooth surfaces with same L_A .

For $\nu \leq 1$, the smooth surfaces in the $r_0 \rightarrow 0$ limit tend to take a square shape with a nearly flat part that approaches the $r = 0$ line. They approach thus the square surface γ_U in this limit.

Area

The dependence of $\text{Area}(\gamma_U)$ as a function of the strip width L_A is shown in Fig. 5. When the surface stays near the brane, we have $r_0 \sim r_b$ and the linear relation (4.7) appears. This holds true both when $\nu \leq 1$ and for the smaller smooth surface when $\nu > 1$.

Let us study the $r_b \gg r_0$ limit. For $\nu = 0$ and $d = 2$ (i.e. AdS_3), $\text{Area}(\gamma_U)$ grows logarithmically when $r_b \gg r_0$.¹² In contrast, in all other cases, i.e. for any $\nu \neq 0$ or $d \geq 2$, the area reaches a finite value given by $\text{Area}(\gamma_U)|_{r_0 \rightarrow 0} = \frac{2A_{d-2}}{(d-2+\nu^2)\eta} \frac{r_b^{d-2}}{L^{d-2}}$. At first order we obtain the asymptotic form valid for $r_0 \ll r_b$,

$$\frac{\text{Area}(\gamma_U)}{A_{d-2}} \frac{(d-1)L^{d-2}}{r_b^{d-2}} \simeq \begin{cases} \frac{2}{\eta\bar{\nu}^2} + \frac{\sqrt{\pi}\Gamma\left(-\frac{\bar{\nu}^2}{2}\right)}{\eta\Gamma\left(\frac{1}{2}(1-\bar{\nu}^2)\right)} \left[\frac{\eta(d-1)\Gamma\left(\frac{1}{2}(3-\bar{\nu}^2)\right)}{\sqrt{\pi}\Gamma\left(1-\frac{\bar{\nu}^2}{2}\right)} \frac{r_b}{L} L_A \right]^{\frac{\bar{\nu}^2}{\bar{\nu}^2-1}} & \text{if } \bar{\nu}^2 < 2 \\ \frac{2}{\eta\bar{\nu}^2} + \frac{\eta(d-1)^2(\bar{\nu}^2-2)r_b^2}{4L^2} L_A^2 & \text{if } \bar{\nu}^2 > 2 \end{cases} \quad (4.18)$$

These expressions are obtained by integrating Eqs. (B.2) from r_0 to r_b , then solving for r_0 as a function of L_A using the $r_b \gg r_0$ approximation. In the $\nu > 1$ case, these expressions describe the area of the large surfaces.

¹²For AdS_3 , $\text{Area}(\gamma_U) \approx \frac{2}{\eta} \log\left(\frac{\eta L_A r_b}{L}\right)$ in the $r_b \gg r_0$ limit. Using that $\eta|_{\nu=0}$ is the inverse AdS radius, and going to Poincaré coordinates using $z = \frac{L}{\eta r}$, the familiar result from e.g. [109] is recovered, with the AdS boundary cut off at z_b .

From (4.17) we can see that $r_0 \ll r_b$ corresponds to $\frac{\eta r_b L_A}{L} \gg 1$ if $\nu < 1$, and to $\frac{\eta r_b L_A}{L} \ll 1$ if $\nu > 1$. In the limits (4.18), this implies that the second term is always subleading and vanishes when $r_0 \rightarrow 0$. For example, keeping fixed $\frac{\eta r_b}{L}$, $r_0 \rightarrow 0$ corresponds to either $L_A \rightarrow \infty$ for $\nu < 1$ or to $L_A \rightarrow 0$ for $\nu > 1$. The approximations of the areas for $r_0 \sim r_b$ and $r_0 \ll r_b$ are shown in Fig. 5.

In the $\nu = 1$ case, it turns out that it is possible to express the area explicitly as a function of L_A . We find the remarkably simple relation

$$\text{Area}(\gamma_U) = A_{d-2} \frac{2}{\eta(d-1)} \left(\frac{r_b}{L}\right)^{d-2} \sin\left(\frac{(d-1)\eta r_b}{2L} L_A\right). \quad (4.19)$$

The linear dilaton background has other geometric properties that will be further used in a future work. Here we notice that, as it can already be seen from (4.16), L_A is *bounded from above*. The largest allowed L_A , corresponding to the argument being equal to $\pi/2$ in (4.19), is $L_A = \frac{\pi L}{(d-1)\eta r_b}$.

4.4 Holographic Entanglement Entropy in the \mathcal{M}_ν^- background

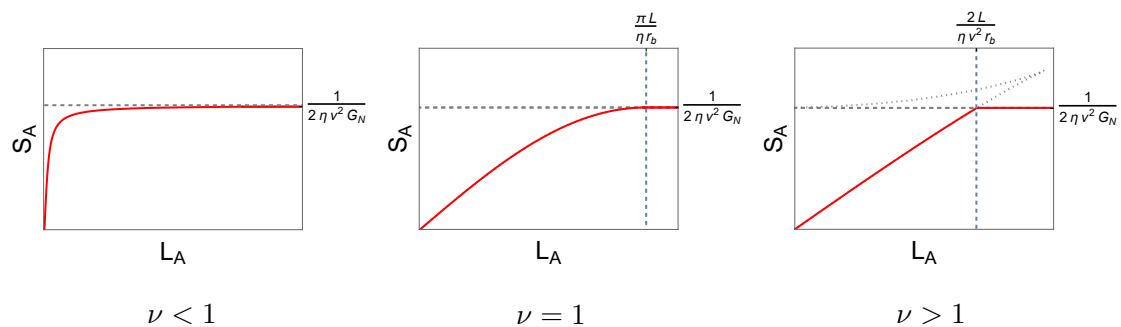


Figure 6. Holographic entanglement entropy from the \mathcal{M}_ν^- background with $d = 2$ spatial dimensions, shown as a function of the strip width. A second order phase transition occurs if $\nu = 1$, while a first order phase transition occurs if $\nu > 1$.

We compute the holographic entanglement entropy of the strip. It turns out that the linear dilaton has, once again, the status of a critical case between two qualitatively different regimes.¹³ The numerical results for the HEE in \mathcal{M}_ν^- assuming $d = 2$ are presented in Fig. 6. A similar qualitative behavior happens for other values of d .

For $\nu < 1$ (and $\nu = 0$ if $d > 2$), we obtain that S_A reaches a plateau at large L_A , with value

$$S_A^{\max} = \frac{A_{d-2}}{2G_N\eta(\nu^2 + d - 2)} \left(\frac{r_b}{L}\right)^{d-2}. \quad (4.20)$$

The existence of HEE plateaux has been noted in the literature, typically at finite temperature, see [114]. Here we observe this saturation phenomenon at *zero temperature*. For

¹³We notice that the large d limit of (4.15) implies $\bar{\nu} \rightarrow 1$. In this limit the minimal surfaces tend to behave effectively as if they were in the linear dilaton background. A related phenomenon pointed out in [122] is that the linear dilaton background appears from general relativity when taking the limit of large number of compactified dimensions.

$d = 2$ the plateau occurs for $\nu > 0$, while for $d > 2$ the plateau occurs for any $\nu \geq 0$, hence even for AdS. From the viewpoint of the general metric (2.2), a HEE plateau occurs when the integral $\int_0^{r_b} dr a(r)^{\frac{d-1}{2}} b(r)$ is finite.

For $\nu = 1$, we know that the base of the smooth surface is bounded from above. This follows from the direct calculations of the area in section 4.3, and from the application of condition (4.12) from the viewpoint of the general warped metric: the upper bound is $\frac{\pi L}{\eta r_b^{(d-1)}}$. There is thus necessarily a phase transition, which happens to occur precisely at this value. Using the explicit formula for the linear dilaton geodesic length (4.19), we find that $S_A^{\nu=1}$ experiences a discontinuity in its second derivative. Therefore there is a *second order* phase transition in the HEE.

For $\nu > 1$ we observe that the base of the geodesics is bounded and that a doubling of the geodesics occurs. From the viewpoint of the general metric, we understand that this phenomenon is a consequence of the curvature singularity that truncates space, see section 4.2. The phase transition occurs when the area of the smaller smooth surface crosses the area of the square surface. We find that this occurs approximately at $L_A \simeq \frac{2L}{\eta(\nu^2+d-2)r_b}$.¹⁴ The first derivative is discontinuous, hence the HEE experiences a *first order* phase transition. In short:

A curvature singularity at finite conformal distance implies
a HEE first order phase transition. (4.21)

The HEE behavior, computed here from the bottom up, closely resembles the one obtained from stringy setups in [65, 72, 74, 76].

5 Stability and the Radion Effective Action

In this section and the next, we study the brane-dilaton system globally. To this end, we put the classical bulk solutions (see [82]) into the fundamental action \mathcal{S} , defined in (2.1). This defines a “holographic” on-shell action that depends only on the brane location r_b and the value of the dilaton on the brane, ϕ_b , $\mathcal{S}_{\text{on-shell}}[r_b, \phi_b]$. We restrict the spacetime dimension to $D = 5$ for simplicity. We remind that we restrict to static configurations, with r_b independent on the spacetime coordinates x^μ , see section 2.3.

5.1 The Effective Potential

At zero-th order in the fluctuations, the on-shell action corresponds to an effective potential $\mathcal{S}_{\text{on-shell}} \equiv - \int d^4x V_{\text{eff}}(r_b, \phi_b)$. In [82] we found

$$V_{\text{eff}} = U_b(\phi_b) \left(\frac{r_b}{L}\right)^4, \quad U_b(\phi_b) = V_b(\phi_b) + \Lambda_b \mp 6M_5^3 \eta(\phi_b), \quad (5.1)$$

¹⁴Notice that this condition depends on the $\frac{\eta r_b L_A}{L}$ combination. This implies that an alternative way to reach the saturation behavior described in (4.20) is to increase r_b at fixed L_A . Namely, for $\nu < 1$, taking large r_b implies $r_b \gg r_0$, which is the limit computed in (4.18). For $\nu > 1$, taking large r_b implies that the square surface necessarily dominates since $L_A \gg \frac{2L}{\eta(\nu^2+d-2)r_b}$ in that limit. Therefore in both cases we have $S = S_A^{\text{max}}$.

for \mathcal{M}_ν^\mp . We introduced the dilaton-dependent scale $\eta(\phi_b) = k e^{\nu \bar{\phi}_b}$, with $\eta(v_b) \equiv \eta$ at the minimum $\phi_b \equiv v_b$.

Stability along the r_b direction requires to tune the 4D cosmological constant to $\Lambda_b = \pm 6M_5^3 \eta$ for \mathcal{M}_ν^\mp . Stability along the ϕ_b direction requires $U_b'' > 0$, which translates as a condition on V_b [82]. In the \mathcal{M}_ν^- spacetime such a vacuum is only metastable since V_{eff} is unbounded from below at large ϕ_b . We will see in section 6.2 that this feature is exacerbated in the presence of a very large black hole.

5.2 The Radion

Both the dilaton and spacetime can fluctuate around the configuration determined by (r_b, v_b) . Upon gauge fixing, these scalar fluctuations reduce to a single degree of freedom, usually called the *radion* field (see [82, 97]). It was shown in [82] that the radion spectrum in \mathcal{M}_ν^\pm always contains an isolated mode $R_0(x)$, that we refer to as *the* radion mode. The rest of the radion spectrum may be either discrete or continuous depending on ν , see summary table 1. Notice that this is tied to the singularity being either at finite or infinite conformal distance.

5.2.1 Definition

We consider the fluctuation of the dilaton and of the scalar sector of the fluctuations of the metric. In conformal coordinates, upon gauge-fixing (see [82, 97]) the following parametrization can be used:

$$ds^2 = e^{-2A(z)} \left[e^{-2F(x,z)} \eta_{\mu\nu} dx^\mu dx^\nu + (1 + 2F(x,z))^2 dz^2 \right],$$

$$\bar{\Phi}(x,z) = \bar{\phi}(z) + \bar{\varphi}(x,z). \quad (5.2)$$

It was shown in [82] that the equations of motion relate the dilaton fluctuation $\varphi(x,z)$ to the $F(x,z)$ fluctuation by

$$\bar{\phi}'(z) \bar{\varphi}(x,z) = (\partial_z - 2A'(z)) F(x,z). \quad (5.3)$$

We introduce a spectral decomposition over an orthogonal basis of modes

$$F(x,z) = \sum_\lambda F_\lambda(z) R_\lambda(x), \quad \text{and} \quad \varphi(x,z) = \sum_\lambda \varphi_\lambda(z) R_\lambda(x), \quad (5.4)$$

where each profile $F_\lambda(z)$ satisfies the equation of motion with mass $p^2 = -m_\lambda^2$. We use $\lambda = 0$ to label the isolated radion mode of our interest, with profile $F_0(z)$ and mass m_0 . The summation over modes in Eq. (5.4) may be either discrete or continuous [82].

5.2.2 Radion profile

The fluctuation in mixed position-momentum space is defined by the 4D Fourier transform

$F(x^\mu, z) = \int \frac{d^4 p}{(2\pi)^4} e^{ip_\mu x^\mu} F(p, z)$. The equation of motion for the profile $F_\lambda(z)$ is [32, 82, 97]

$$\partial_z^2 F_\lambda(z) + \frac{1+2\nu^2}{\nu^2-1} \frac{1}{z} \partial_z F_\lambda(z) + m_\lambda^2 F_\lambda(z) = 0. \quad (5.5)$$

$F_\lambda(z)$ satisfies the following boundary conditions:

- i) Regularity at $z = 0$ if $z \in (0, z_b]$, or at $z \rightarrow \infty$ if $z \in [z_b, \infty)$.
- ii) Boundary condition at the brane [82]:

$$\left(\partial_z - 2A'(z) \mp \frac{2m_\lambda^2 e^A}{U_b''} \right) F_\lambda(z) \Big|_{z=z_b} = 0, \quad (5.6)$$

where the $-$ sign stands for $z \in (0, z_b]$, i.e. for $\mathcal{M}_{\nu < 1}^+$ and $\mathcal{M}_{\nu > 1}^-$, and the $+$ sign stands for $[z_b, \infty)$, i.e. for $\mathcal{M}_{\nu < 1}^-$ and $\mathcal{M}_{\nu > 1}^+$. This boundary condition is generated by the brane terms in the action (2.1), as discussed in e.g. Ref. [97].

Eq. (5.6) constitutes the eigenvalue equation whose solution for the lightest mode m_0 corresponds to the radion mass. Solving for a small mass $m_0 \ll \eta$ we find the profiles corresponding to the radion mode R_0 ,

$$F_0(z) \simeq \begin{cases} C_F \left(\frac{z}{z_b}\right)^{2\gamma} & \text{in } \mathcal{M}_\nu^+ \\ C_F \left(1 + \frac{m_0^2}{4(\gamma-1)} z^2\right) & \text{in } \mathcal{M}_\nu^- \end{cases}, \quad (5.7)$$

and

$$\varphi_0(z) \simeq \begin{cases} \sqrt{3M_5^3} C_F \nu \left(\frac{z}{z_b}\right)^{2\gamma} & \text{in } \mathcal{M}_\nu^+ \\ -2\sqrt{3M_5^3} \frac{C_F}{\nu} \left(1 - \frac{\nu^2-1}{6} m_0^2 z^2\right) & \text{in } \mathcal{M}_\nu^- \end{cases}. \quad (5.8)$$

The normalization constant is determined by substituting the solutions in the on-shell action and requiring canonical normalization,

$$S_{R_0, \text{kin}} = - \int d^4 x dz e^{-3A(z)} (6M_5^3 |F_0(z)|^2 + |\varphi_0(z)|^2) (\partial_\mu R_0)^2 \equiv -\frac{1}{2} \int d^4 x (\partial_\mu R_0)^2, \quad (5.9)$$

which sets

$$C_F = \begin{cases} \frac{|1-\nu^2|}{\sqrt{2}} \frac{\eta^{3/2} z_b}{\sqrt{3M_5^3}} & \text{in } \mathcal{M}_\nu^+ \\ \frac{\nu|1-\nu^2|}{2} \frac{\eta^{3/2} z_b}{\sqrt{3M_5^3}} & \text{in } \mathcal{M}_\nu^- \end{cases}. \quad (5.10)$$

While the determination of C_F is relevant for canonical normalization, it is of course not necessary for calculating the radion mass.

5.3 Radion Mass from the On-Shell Action

We show how to compute the radion mass directly from the on-shell action. This provides an important consistency check of the equation of motion and boundary condition (5.5), (5.6), from which the mass can be independently derived. This is also a necessary step

to further derive the radion effective action, including its interactions with other quantum fields. The full radion quadratic action is

$$\mathcal{S}_{R_0} = - \int d^4x \left[\frac{1}{2} (\partial_\mu R_0(x))^2 + \frac{1}{2} m_0^2 R_0^2(x) \right]. \quad (5.11)$$

To obtain the radion mass term we first rewrite the full renormalized on-shell action as

$$\mathcal{S}_{\text{on-shell}} = \mathcal{S}_{\text{bulk}}^{\text{ren}} + \mathcal{S}_{\text{brane}} + \mathcal{S}_{\text{GHY}}, \quad (5.12)$$

with

$$\mathcal{S}_{\text{bulk}}^{\text{ren}} = \int d^5x \sqrt{g} \left(\frac{M_5^3}{2} {}^{(5)}R - \frac{1}{2} (\partial_M \phi)^2 - V(\phi) \right) + \mathcal{S}_{\text{ct}}, \quad (5.13)$$

$$\mathcal{S}_{\text{brane}} = - \int_{\text{brane}} d^4x \sqrt{\bar{g}} (V_b(\phi_b) + \Lambda_b), \quad (5.14)$$

$$\mathcal{S}_{\text{GHY}} = M_5^3 \int_{\text{brane}} d^4x \sqrt{\bar{g}} K. \quad (5.15)$$

The integral in \mathcal{M}_ν^+ is infinite. We regularize it with a counterterm given by [82, 123]

$$\mathcal{S}_{\text{ct}} = 2M_5^3 \int_\Sigma d^4x \sqrt{h} \eta(\phi_\Sigma), \quad (5.16)$$

with Σ a 4D cutoff surface located at $r_\Sigma \gg r_b$, and $h_{\mu\nu}$ being the induced metric on Σ . The counterterm receives contributions from the bulk, and also from the boundary due to the GHY term at r_Σ .

We expand the action at quadratic order in the radion field $R(x)$. Notably, the expansion of the metric determinant is

$$g \equiv |\det g_{MN}| = e^{-5A(z)} \left(1 - 2F(x, z) - \frac{5}{2} F^2(x, z) + \dots \right). \quad (5.17)$$

Focussing on the radion mode R_0 , we substitute the expressions of the F_0, φ_0 profiles (5.7) and (5.8) in the renormalized on-shell action. We find the following contributions to the R_0^2 term:

$$\mathcal{S}_{\text{bulk, mass}}^{\text{ren}} = \begin{cases} \frac{16-24\nu^2-3\nu^4}{6(1-\nu^2)^2} \frac{1}{z_b^2} \int d^4x R_0^2(x) & (\mathcal{M}_\nu^+) \\ -\frac{13}{3} \frac{\nu^2}{(1-\nu^2)^2} \frac{1}{z_b^2} \int d^4x R_0^2(x) & (\mathcal{M}_\nu^-) \end{cases}, \quad (5.18)$$

$$\mathcal{S}_{\text{brane, mass}} = \begin{cases} -\frac{U_b'' \nu^2 - 2\eta(4-\nu^2)^2}{4(1-\nu^2)^2} \frac{1}{\eta z_b^2} \int d^4x R_0^2(x) & (\mathcal{M}_\nu^+) \\ -\frac{U_b'' + 18\nu^2 \eta}{2(1-\nu^2)^2} \frac{1}{\eta z_b^2} \int d^4x R_0^2(x) & (\mathcal{M}_\nu^-) \end{cases}, \quad (5.19)$$

$$\mathcal{S}_{\text{GHY, mass}} = \begin{cases} -\frac{8}{3} \frac{(4-3\nu^2)}{(1-\nu^2)^2} \frac{1}{z_b^2} \int d^4x R_0^2(x) & (\mathcal{M}_\nu^+) \\ \frac{40}{3} \frac{\nu^2}{(1-\nu^2)^2} \frac{1}{z_b^2} \int d^4x R_0^2(x) & (\mathcal{M}_\nu^-) \end{cases}. \quad (5.20)$$

We have made use of the following identities

$$V_b(v_b) = 0, \quad V_b'(v_b) = \pm 2\sqrt{3M_5^3\nu\eta}, \quad V_b''(v_b) = U_b''(v_b) \pm 2\nu^2\eta, \quad \Lambda_b = \pm 6M_5^3\eta, \quad (5.21)$$

for \mathcal{M}_ν^\mp . The first condition is a choice with no loss of generality. The second and third conditions follow from the definition of the brane-localized effective potential $U_b(\phi_b)$ given in (5.1), using that U_b has a minimum at $\phi_b = v_b$. The fourth condition corresponds to the tuning that ensures $U_b(v_b) = 0$, so that the effective radion potential $V_{\text{eff}}(r_b, v_b) = U_b(v_b) \left(\frac{r_b}{L}\right)^4$ has a flat direction in r_b .

The full mass term is then

$$\mathcal{S}_{R_0, \text{mass}} = \begin{cases} -\frac{\nu^2}{4(1-\nu^2)^2} U_b'' \frac{1}{\eta z_b^2} \int d^4x R_0^2(x) & (\mathcal{M}_\nu^+) \\ -\frac{1}{2(1-\nu^2)^2} U_b'' \frac{1}{\eta z_b^2} \int d^4x R_0^2(x) & (\mathcal{M}_\nu^-) \end{cases}. \quad (5.22)$$

From comparison with Eq. (5.11), we identify the radion mass

$$m_0^2 = \begin{cases} \frac{\nu^2}{2(1-\nu^2)^2} U_b'' \frac{1}{\eta z_b^2} & (\mathcal{M}_\nu^+) \\ \frac{1}{(1-\nu^2)^2} U_b'' \frac{1}{\eta z_b^2} & (\mathcal{M}_\nu^-) \end{cases}. \quad (5.23)$$

This result agrees with the pole mass obtained from the radion propagator [33, 82, 124]

$$iG_F(z, z'; p^2) = \sum_\lambda \frac{F_\lambda(z) F_\lambda^*(z')}{p^2 + m_\lambda^2 - i\varepsilon} \quad (5.24)$$

in the limit of small U_b'' . We have similarly checked the mass term at next-to-leading order in the U_b'' expansion, finding again consistency with the result from [82].

6 Holographic Thermal Phase Transitions

We turn to the on-shell action in the presence of the bulk black hole. As discussed in Ref. [82], the black hole is always in the \mathcal{M}_ν^- region. We use the (x^μ, r) coordinates with $r \in (0, r_b]$. Throughout this section we use a Z_2 orbifold convention as in [93] which implies that the spacetime is mirrored on the other side of the brane. The domain of integration of r is thus doubled in the action. A notable implication is that the entropy of the black hole horizon is doubled when using this convention, see e.g. Ref. [61].

The black hole metric is given in (2.15). We assume that the brane is outside the black hole, $r_h < r_b$. We define $f(r_b) \equiv f_b$, with $f(r) = 1 - \left(\frac{r_h}{r}\right)^{4-\nu^2}$. We introduce the brane proper time $dt = \frac{r_b}{L} \sqrt{f(r_b)} d\tau$, with τ the comoving time from the comoving volume element $d^4x = d\tau d^3x$.

We find the on-shell action

$$\mathcal{S}_{\text{on-shell}} = - \int dt d^3x \left(\frac{r_b}{L}\right)^3 U_b(\phi_b), \quad U_b(\phi_b) = U_b^0(\phi_b) + 6M_5^3\eta(\phi_b)\Delta(r_b, r_h), \quad (6.1)$$

with

$$\Delta(r_b, r_h) = \frac{1}{\sqrt{f_b}} \left(\sqrt{f_b} - 1 + \frac{(2 + \nu^2)}{6} (1 - f_b) \right). \quad (6.2)$$

The $U_b^0(\phi_b)$ term in (6.1) is $U_b^0(\phi_b) = U_b(\phi_b)|_{r_h \rightarrow 0}$, i.e. it is the brane-localized effective potential with no black hole given in (5.1). The effect of the black hole is fully encoded into the second term.

6.1 Thermodynamics on the Brane

From the viewpoint of the brane, the black hole contributes as a *perfect fluid*, see [27, 34, 35, 82]. It was shown in [82] that the thermodynamics of this holographic fluid essentially mirrors the bulk black hole thermodynamics.

Volume

A first thermodynamic variable defined on the brane is the volume (V_b), which is related to the comoving volume $V_3 = \int d^3x$ by

$$V_b \equiv V_3 a^3(r_b), \quad (6.3)$$

with the scale factor

$$a(r_b) \equiv e^{-A(r_b)} = \frac{r_b}{L}. \quad (6.4)$$

Temperature

The fluid temperature (T_b) is related to the Hawking temperature T_h as [82]

$$T_b = \frac{T_h}{a(r_b)} = \frac{4 - \nu^2}{4} \frac{\eta}{\pi} \left(\frac{r_b}{r_h} \right)^{\nu^2 - 1}. \quad (6.5)$$

The Hawking temperature T_h is obtained by requiring the absence of conical singularity near the horizon (see e.g. [35] for the general planar black hole case).

We can notice that T_b decreases (increases) with r_b/r_h for $\nu < 1$ ($\nu > 1$). For $\nu = 1$, the fluid has a constant temperature $T_b|_{\nu=1} = \frac{3\eta}{4\pi}$ whenever it exists.

Free energy

The on-shell action can be expressed in Euclidean time ($t = -it_E$) as $i\mathcal{S}_{\text{on-shell}} = -\mathcal{S}_{\text{on-shell}}^E$. When ϕ_b is at its vev v_b^T , we identify the free energy of the system: ¹⁵

$$\mathcal{S}_{\text{on-shell}}^E \Big|_{\phi_b=v_b} \equiv \beta V_b F. \quad (6.6)$$

Here F is the free energy density and $\beta = \frac{1}{T}$ the inverse temperature of the system.

¹⁵Notice that in the presence of a black hole, the vev (v_b^T) is different from the vev with no black hole (v_b), and thus $U_b^0 \equiv U_b^0(v_b^T)$ is generically non-vanishing in the former case. Nevertheless, this effect is small for r_b large enough compared to r_h , as can be seen in Fig. 8.

At equilibrium, we have $T = T_b$ as imposed by the absence of conical singularity upon Euclidean time compactification. In this section we will briefly discuss the out-of-equilibrium case of $T \neq T_b$, in which case the free energy has an extra contribution $F_{\text{cone}} \propto (T - T_b)$ [62, 125]. The T_b temperature can be identified even in case of non-vanishing conical singularity, see [125].

The free energy of the system is given by

$$F = U_b^0 + F_{\text{fluid}} + F_{\text{cone}}, \quad F_{\text{fluid}} = 6M_5^3 \eta \Delta(T_b), \quad (6.7)$$

with $\Delta(T_b) \equiv \Delta(r_b, r_h)$. In the small black hole limit $r_h \ll r_b$, the fluid free energy density simplifies to

$$F_{\text{fluid}} \Big|_{r_h \ll r_b} \approx -(1 - \nu^2) \eta M_5^3 \left(\frac{r_h}{r_b} \right)^{4 - \nu^2}. \quad (6.8)$$

This reproduces the result presented in [82]. In this limit the free energy is negative for $\nu < 1$ and positive for $\nu > 1$. We will see in section 6.2 that this is not true away from the small r_h limit, which will be the cause of a phase transition. In contrast, (6.2) implies that the vanishing of F_{fluid} for $\nu = 1$ remains exact for any r_h .

A typical out-of-equilibrium situation is when a thermal bath with temperature T is localized on the brane, while the black hole/holographic fluid has $T_b \ll T$. The thermal bath radiates into the bulk, feeding the out-of-equilibrium black hole. In such a setup the bulk is non-empty, and a Vaidya-type metric has to be used [95, 96]. Here we will discuss this case only qualitatively.

6.2 Phase Transitions

The information about phase transitions is encoded into the $\Delta(T_b)$ function. A phase with no fluid, i.e. with no black hole ($r_h \rightarrow 0$), has $f_b|_{r_h \rightarrow 0} = 1$ and thus $\Delta(T_b)|_{r_h \rightarrow 0} = 0$. The existence of phase transitions is thus controlled by the sign of $\Delta(T_b)$.

Critical temperature. The critical value of T_b at which a phase transition occurs is denoted by T_c and is determined by $\Delta(T_c) = 0$. Written in terms of f_b , the solutions are given by

$$\sqrt{f_{b\pm}} = \frac{3 \pm |\nu^2 - 1|}{2 + \nu^2}. \quad (6.9)$$

We also know that physical solutions must satisfy $f_b \leq 1$.

Latent heat. The order of the phase transition is controlled by the associated latent heat per unit volume, ℓ_b . The transition is first order if $\ell_b \neq 0$ and second order if $\ell_b = 0$. The latent heat for a phase transition at temperature T_c is defined as $L_b = T_c \Delta S$. The entropy in each phase satisfies $S = -\partial(V_b F)/\partial T_b$. If r_b is large enough compared to r_h (typically $r_b \gtrsim 1.1 r_h$) then $v_b^T \simeq v_b$, and the difference between the two phases is only due to the fluid free energy, which furthermore vanishes identically in the phase with no black hole. Putting the pieces together and using the chain rule, we derive the latent heat for the transition from the no black hole phase to the black hole phase at a given critical

temperature T_c via

$$\ell_b = -T_c \frac{\partial F_{\text{fluid}}}{\partial r_b} \frac{\partial r_b}{\partial T_b} \Big|_{r_b, c}. \quad (6.10)$$

Case $\nu < 1$

For $\nu \in [0, 1)$, we have $f_- = 1$ while the other solution gives $f_+ > 1$ for any value of ν , which is not physical. Therefore $\Delta(T_b)$ cannot change sign as a function of T_b . It satisfies $\Delta(T_b) \leq 0$ for all values of T_b , with $\Delta(T_b) \rightarrow 0$ in the limit of no black hole $r_h \rightarrow 0$, for which $T_b \rightarrow 0$.

We conclude that the black hole phase is energetically favored whenever it exists. The critical temperature is thus $T_c = 0^+$. The latent heat vanishes, hence it is a *second order* phase transition.

The $F(T_b)$ curve is pictured in Fig. 7, left panel.

Case $\nu > 1$

For $\nu \in (1, 2)$, we have $f_+ = 1$ and

$$\sqrt{f_-} = \frac{4 - \nu^2}{\nu^2 + 2}, \quad (6.11)$$

which is inside the $[0, 1]$ interval. There is thus a phase transition at a nonzero value of r_h/r_b ,

$$\frac{r_h}{r_b} \Big|_c = \left(\frac{12(\nu^2 - 1)}{(\nu^2 + 2)^2} \right)^{\frac{1}{4-\nu^2}}. \quad (6.12)$$

The corresponding critical temperature is

$$T_b = \frac{4 - \nu^2}{4} \frac{\eta}{\pi} \left(\frac{(\nu^2 + 2)^2}{12(\nu^2 - 1)} \right)^{\frac{\nu^2 - 1}{4 - \nu^2}} \equiv T_c. \quad (6.13)$$

In terms of the horizon position, it turns out that $\Delta(T_b) > 0$ for $r_h < r_{h,c}$ and $\Delta(T_b) < 0$ for $r_h > r_{h,c}$.

We find a latent heat per unit volume that is finite for any $1 < \nu < 2$,

$$\ell_b = -\frac{12(\nu^2 - 1)}{4 - \nu^2} M_5^3 \eta, \quad (6.14)$$

therefore the phase transition is *first order*.

Furthermore, the latent heat is *negative*. This is tied to the fact that for $\nu > 1$, T_b decreases when r_b approaches r_h . This implies that there is a cusp in the free energy curve. This is shown in Fig. 7, right panel.

Case $\nu = 1$

For $\nu = 1$ i.e. the linear dilaton background, the fluid has constant temperature $T_b = \frac{3\eta}{4\pi}$ and vanishing free energy, $F_{\text{fluid}} = 0$, as shown in [27, 82]. That is, the fluid has Hagedorn

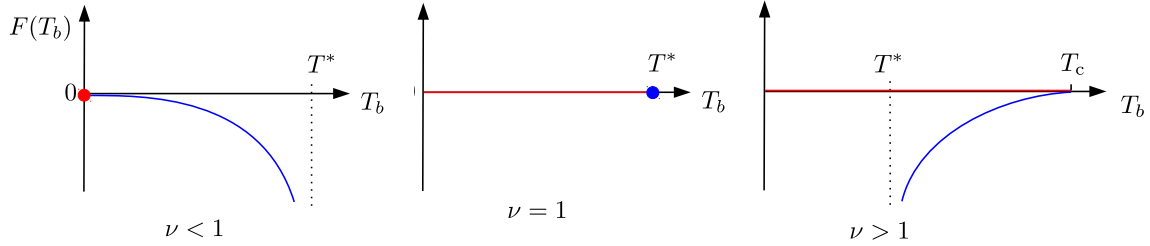


Figure 7. Free energy curves and thermal phases as a function of the temperature of the holographic fluid. Red corresponds to the phase with no black hole, blue corresponds to the black hole phase. The black hole phase is stable at any value of T_b shown on the graph.

behavior. We conclude that the phase transition occurs at $T_c = \frac{3\eta}{4\pi}$ and is of second order. This is shown in Fig. 7, middle panel.

6.3 Discussion

Heat Capacity

We computed the heat capacity at constant volume of the black hole, which is given by $C_V = (\partial E / \partial T_b)_{V_b}$, where E is the energy of the system. We find that the heat capacity is positive at all values for which the black hole phase is energetically favored. Hence the black hole is thermodynamically stable for all values of ν .

Temperature bound

For $\nu < 1$ and $\nu > 1$ the fluid free energy tends to negative infinity when the black hole approaches the brane. In this limit the temperature approaches the finite value

$$T^* = \frac{4 - \nu^2}{4\pi} \eta. \quad (6.15)$$

For $\nu < 1$, T^* is approached from below, i.e. the fluid temperature is constrained to the interval $T_b \in [0, T^*)$. For $\nu > 1$, T^* is instead approached from above, i.e. the fluid temperature is bounded from below, $T_b \in (T^*, \infty)$. Notice that in the $\nu = 1$ case, the temperature is restricted to the single value T^* (see also [126, 127]).

Cosmological scenario

The thermodynamic behavior of the black hole is perhaps more intuitively understood when considering a brane cosmology-type scenario where a thermal bath of temperature $T \gg T_b$ is present on the brane. The thermal bath leaks energy into the bulk, feeding the bulk black hole, which is assumed to not exist initially (see [95, 96, 128] for analyses of such scenarios in AdS). The rigorous evolution of such cosmological scenarios is done using a Vaidya-type metric. Here we discuss them only qualitatively to get a sense of the black hole behavior.

For $\nu < 1$ and $\nu = 1$, the black hole is created via a second order phase transition whenever some energy leaks into the bulk. For $\nu < 1$ the temperature grows while the

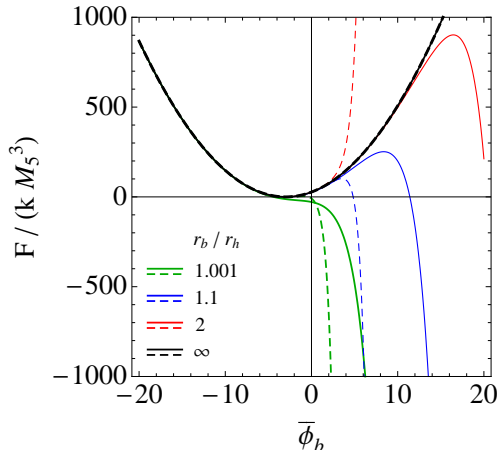


Figure 8. The total free energy density as a function of $\bar{\phi}_b$, assuming the brane-localized effective potential $V_b(\phi_b) = \frac{\gamma}{2}(\phi_b - v_b)^2$. Solid (dashed) lines are for $\nu = 0.5$ (1.5). We have considered $\bar{v}_b = -3$ and $\gamma = 2k$. Unstability of the system occurs when the horizon comes close to the brane.

black hole size increases. For $\nu = 1$ the temperature is instead constant and non zero for any black hole size, since it is independent of r_h .

For $\nu > 1$, the thermal bath should heat up the bulk sufficiently such that a first order phase transition occurs and the black hole directly forms with finite size given by (6.12).¹⁶ The black hole temperature decreases as its size increases further.

6.4 Instability from Big Black Holes

We study the stability of the brane-dilaton system in the presence of the black hole. This is described by the brane-localized effective potential $U_b(\phi_b)$ given in (6.1). Notice that this is equivalent to study the free energy at $\phi_b \neq v_b$.

The stabilization of ϕ_b is driven by the brane potential $V_b(\phi_b)$, see (5.1). At zero temperature, due to the ϕ_b dependence of η , requiring $U_b''(v_b) > 0$ implies the stability condition $V_b''(v_b) > 2\nu^2\eta$ [82].

At finite temperature, the extra contribution from the black hole in (6.7) is also proportional to $\eta(\phi_b)$. In the black hole phase this term is negative, since by definition we have $\Delta(r_b, r_h) < 0$ for the black hole phase to be energetically favored.

When the black hole becomes so big that its horizon approaches the brane, $r_h \sim r_b$, the effect of the black hole dominates and we have $\Delta(r_b, r_h) \sim -\frac{4-\nu^2}{6\sqrt{f_b}}$ with f_b approaching zero. Therefore this black hole term tends to *destabilize* the effective potential. The critical value for r_h/r_b depends on the steepness of the U_b potential, and is approximately given by

$$\frac{r_h}{r_b} \approx 1 - \frac{\nu^4}{9} \frac{4 - \nu^2}{(U_b^{0''}(v_b^T))^2} \eta^2(v_b^T). \quad (6.16)$$

¹⁶The first order phase transition may proceed via bubble nucleation and thus produces gravitational waves, see e.g. [61, 63, 64, 125, 129, 130].

Value of ν	0 [AdS]	(0, 1)	1 [LD]	$(1, \sqrt{d})$	\sqrt{d}
Singularity	✗	good			bad
Brane-singularity conf. distance	✗	∞		finite	
Timelike boundary	✗			✓	
Bulk Black hole	✓				✗
Gravity spectrum ($D \geq 4$)	continuum		gapped cont.	discretum	
Confinement	✗		✓		
Thermal phase transition ($D = 5$)	second order			first order	
Entanglement phase transition	✗		second order	first order	

Table 1. *Properties of the \mathcal{M}_ν^- spacetime. The first block reviews global features, the second block summarizes key holographic properties.*

Notice that in the stiff potential limit $U_b^{0''} \rightarrow \infty$, the horizon can reach the brane since the potential cannot be destabilized.

We conclude that, for finite $U_b^{0''}$, the T^* temperature cannot be actually reached. A radical change in the system occurs for a value of r_h slightly below r_b : the classical effective potential for ϕ_b becomes unbounded from below — and can only get stabilized at loop level. Numerical examples of this effect are presented in Fig. 8, where we used $V_b(\phi_b) = \frac{\gamma}{2}(\phi_b - v_b)^2$.

7 Summary

In this paper we studied holographic entanglement entropy and revisited thermal phase transitions and confinement in dilaton gravity, with special emphasis on their interplay with bulk curvature singularities.

We mostly focus on a very simple class of backgrounds \mathcal{M}_ν , parameterized by a real parameter ν interpolating AdS ($\nu = 0$) and linear dilaton ($\nu = 1$), that retains the essence of the phenomena we want to highlight. We also prove some properties in general warped metrics. The considered backgrounds are non-asymptotically AdS and feature a flat brane on which the holographic theory is defined. Curvature singularities can be either at infinite or finite conformal distance from the brane. We show that the latter case is automatically implied by a metric zero at finite conformal distance, in which case the singularity acts as a regular boundary that truncates spacetime.

We show that the behaviors of the entanglement, thermodynamics, and confinement properties are all tied to the nature of the bulk singularity. Some important results are summarized in Tab. 1.

Confinement

We first revisit the notion of holographic confinement based on classical strings. In our background the behavior of the string is straightforwardly understood. We show that for $\nu < 1$ ($\nu > 1$) the string bends towards small (large) r , while it is straight for $\nu = 1$.

An equivalent coordinate-free statement is that the string living in the \mathcal{M}_ν background is repelled from the string frame curvature singularity.

We further show that, when attached to the boundary/brane on which the dual theory is defined, the string is forced to have a straight profile for $\nu > 1$. The resulting picture is that the theory is not confining for $\nu < 1$, while it is perfectly confining for both $\nu = 1$ (linear dilaton) and $\nu > 1$, in each case with the same string tension. We show that this picture provides an intuitive understanding of holographic confinement in asymptotically-AdS backgrounds.

Entanglement Entropy

Having a solid understanding of the confinement criterion, we turn to holographic entanglement entropy. We consider a $d - 1$ strip localized on the brane at given time. Two kinds of surfaces anchored to the boundary of the strip are possible: a smooth surface and a square one that reaches the singularity.

Working first with a general warped metric, we show that a metric zero at finite conformal distance implies that the square surface has finite area and ends on the curvature singularity. We point out that a necessary condition for HEE phase transition to occur is that the width of the smooth surface's base be bounded from above. We determine a sufficient condition for this to occur, that relies on the existence of a singularity at finite conformal distance. We show that for such a singularity, there exist necessarily two smooth surfaces of different areas anchored to a given strip. This implies that the HEE phase transition is first order in this case.

These phenomena are explicitly shown to occur in the \mathcal{M}_ν^- background. The base of the smooth surface is bounded from above for $\nu \geq 1$, and for $\nu > 1$ two different smooth surfaces exist. This confirms that the doubling phenomenon is tied to the existence of a singularity at finite conformal distance. We derive approximate formulas for the areas of the smooth surfaces in the generic dilaton gravity background. We also find an exact formula for the area in the linear dilaton background.

For $\nu < 1$ the smooth surface has minimal area for any width of the strip. In this case the entanglement entropy reaches a plateau at large strip width for $\nu \geq 0$ if $d > 2$ and for $\nu > 0$ if $d = 2$.

For $\nu = 1$, the entanglement entropy features a transition between the smooth surface and the square surface at finite strip width. From our exact formula for the smooth surface in the linear dilaton background, we find that a discontinuity occurs at second order. Hence the linear dilaton stands out once again as a special, critical, case.

For $\nu > 1$, there are two smooth surfaces and the square one. A transition between the smooth surface of smaller area and the square surface occurs at finite strip width. The transition turns out to be of first order. The behavior of the areas and of the transition closely resembles that obtained from stringy setups in [65, 72, 74, 76]. In our setup we find that this characteristic behavior is tied to the curvature singularity being at finite conformal distance.

Thermodynamics and Stability

We compute the on-shell effective action of the system with no black hole (i.e. at zero temperature) as a function of the classical value of the dilaton field and of the brane position. Upon gauge fixing of spacetime fluctuations, the scalar fluctuations reduce to a single degree of freedom, the radion. We derive the radion profile and compute the full quadratic action of the radion, which completes and cross checks the results from [82]. Under a certain condition on the brane-localized potential, the radion is massive, which ensures stability of the system.

The existence of the planar black hole amounts, from the viewpoint of the brane, to the existence of a perfect fluid. We study the thermodynamics of this fluid, including phase transitions, extending the results from [82].

We show that for $\nu \leq 1$ the fluid/black hole appears via a second order phase transition whenever the temperature is nonzero. In contrast, for $\nu > 1$, the black hole appears above a nonzero critical temperature via a first order phase transition. In the linear dilaton case $\nu = 1$, the black hole has always the same nonzero temperature, but appears via a second order phase transition.

Remarkably, the order of these thermal phase transitions matches the one of the entanglement entropy phase transitions.

In the black hole phase considered, the black hole is always thermodynamically stable in the sense of having positive heat capacity. The black hole temperature increases with its size for $\nu < 1$, while it decreases with its size for $\nu > 1$, which causes the latent heat to be negative. The black hole temperature admits an upper bound for $\nu < 1$, and a lower bound for $\nu > 1$, which is tied to the brane not being engulfed by the horizon.

We demonstrate that, in the extreme situation where the horizon approaches the brane, a dramatic instability in the dilaton vev occurs, that makes the classical effective potential unbounded from below.

Acknowledgments

We thank Matti Järvinen, Javier Subils, Miguel Ángel Vázquez-Mozo and collaborators for their valuable correspondence, and Lucas de Souza for insightful comments regarding App. A. The work of EM is supported by the project PID2020-114767GB-I00 and by the Ramón y Cajal Program under Grant RYC-2016-20678 funded by MCIN/AEI/10.13039/50-1100011033 and by “FSE Investing in your future”, by Junta de Andalucía under Grant FQM-225, and by the “Prórrogas de Contratos Ramón y Cajal” Program of the University of Granada. The work of MQ is supported by the grant PID2023-146686NB-C31 funded by MICIU/AEI/10.13039/501100011033/ and by FEDER, EU. IFAE is partially funded by the CERCA program of the Generalitat de Catalunya.

A Derivation of Property (2.18)

We prove Prop. (2.18). The essence of the derivation is to show that, using the mean value theorem, any interval in the vicinity of the metric zero contains a point such that $a'(z)/a(z)$ is singular, no matter how small the interval is. We make the hypothesis that $a'(z)/a(z)$ is *strictly monotonic* near the singularity.

The mean value theorem states that for any function $a(z)$ continuous on $[z_1, z_2]$ and differentiable on (z_1, z_2) there is at least one point z_{12} in (z_1, z_2) such that

$$\log a(z_2) - \log a(z_1) = \frac{a'(z_{12})}{a(z_{12})}(z_2 - z_1). \quad (\text{A.1})$$

We apply the theorem in the vicinity of the metric zero, $a(z_s) = 0$. Following the convention from section 4.2, spacetime is defined to the right of z_s , $z \geq z_s$. We place the small closed interval to the right of the metric zero, and take the limit $z_1 \rightarrow z_s^+$ in (A.1).

To ensure that z_{12} converges when taking the limit $z_1 \rightarrow z_s^+$, we implement this limit using a discrete sequence as follows. Define $z_1 \equiv z_s + \frac{1}{n}$, where $n \in \mathbb{N}$ starts at a value larger than $\frac{1}{z_2 - z_s}$ and is taken to infinity. For each n there is a value of z_{12} , denoted $z_{12} \equiv z(n, z_2) = z_n$. Since $z_n \in (z_s, z_2)$, (z_n) is a bounded sequence. Thus the Bolzano-Weierstrass theorem ensures that there exists a subsequence $(z_{n_j}) \equiv (\hat{z}_j)$ of (z_n) that is convergent, i.e. $\lim_{j \rightarrow \infty} \hat{z}_j = \hat{z}$, with $\hat{z} = \hat{z}(z_2)$.

Starting from (A.1), we have

$$\lim_{j \rightarrow \infty} \frac{a'(\hat{z}_j)}{a(\hat{z}_j)} = \lim_{z \rightarrow \hat{z}} \frac{a'(z)}{a(z)} = \lim_{j \rightarrow \infty} \frac{\log a(z_2) - \log a(z_s + n_j^{-1})}{z_2 - z_s - n_j^{-1}} = \infty, \quad (\text{A.2})$$

since $\log(a(z))$ diverges at z_s while by assumption z_s is finite. That is, there is at least one point \hat{z} in (z_s, z_2) for which $a'(z)/a(z)$ is infinite. The assumption that $a'(z)/a(z)$ is strictly monotonic on the interval (z_s, z_2) implies that $\log(a(z))$ is strictly concave or convex, which ensures that the intermediate point \hat{z} is unique.

We can then approach z_2 to z_s^+ , such that the intermediate point $\hat{z}(z_2)$ is forced to tend to z_s^+ . Taking this limit in (A.2), we obtain

$$\lim_{z_2 \rightarrow z_s^+} \frac{a'(\hat{z}(z_2))}{a(\hat{z}(z_2))} = \lim_{\hat{z} \rightarrow z_s^+} \frac{a'(\hat{z})}{a(\hat{z})} = \infty. \quad (\text{A.3})$$

This proves Prop. (2.18).

B Minimal Surfaces and Geodesics

We demonstrate that the equations for the smooth minimal surfaces anchored to the strip in \mathcal{M}_ν can be mapped onto geodesic equations in $\mathcal{M}_{\bar{\nu}}$. From (4.3) and (4.4), substituting

the metric factors in Einstein frame (2.7), we obtain

$$\frac{d\text{Area}(\gamma_U)}{dr} = \frac{2A_{d-2}}{\eta r_b^{\nu^2} L^{d-2}} \frac{r^{2(d-2)+\nu^2}}{\sqrt{r^{2(d-1)} - r_0^{2(d-1)}}}, \quad \frac{du}{dr} = \frac{r_0^{d-1} L}{\eta r_b^{\nu^2}} \frac{r^{\nu^2-2}}{\sqrt{r^{2(d-1)} - r_0^{2(d-1)}}}. \quad (\text{B.1})$$

These expressions closely resemble the differential equations for geodesics in \mathcal{M}_ν spacetime:

$$\frac{ds}{dr} = \frac{2}{\eta r_b^{\nu^2}} \frac{r^{\nu^2}}{\sqrt{r^2 - r_0^2}}, \quad \frac{dx}{dr} = \frac{r_0 L}{\eta r_b^{\nu^2}} \frac{r^{\nu^2-2}}{\sqrt{r^2 - r_0^2}}, \quad (\text{B.2})$$

being s the geodesic length. By introducing the change of variable $y = r^{d-1}$, we explicitly relate the two sets of equations. Under this transformation, the minimal surface equations (B.1) are related to the geodesic ones (B.2) by

$$\frac{d\text{Area}(\gamma_U)}{dy} = \frac{A_{d-2}}{d-1} \left(\frac{r_b}{L}\right)^{d-2} \frac{ds}{dy} \Big|_{\nu \rightarrow \bar{\nu}}, \quad \frac{du}{dy} = \frac{r_b^{d-2}}{d-1} \frac{dx}{dy} \Big|_{\nu \rightarrow \bar{\nu}}, \quad (\text{B.3})$$

where

$$\bar{\nu}^2 = 1 + \frac{\nu^2 - 1}{d-1}. \quad (\text{B.4})$$

For example, the minimal surfaces anchored to the strip in AdS_{d+1} are related to the geodesics of $\mathcal{M}_{\bar{\nu}}$ by $\bar{\nu}^2 = \frac{d-2}{d-1}$.

References

- [1] O. Aharony, S. S. Gubser, J. M. Maldacena, H. Ooguri, and Y. Oz, *Large N field theories, string theory and gravity*, *Phys. Rept.* **323** (2000) 183–386, [[hep-th/9905111](#)].
- [2] A. Zaffaroni, *Introduction to the AdS-CFT correspondence*, *Class. Quant. Grav.* **17** (2000) 3571–3597.
- [3] J. Kaplan, “Lectures on AdS/CFT from the Bottom Up.” <https://sites.krieger.jhu.edu/jared-kaplan/files/2016/05/AdSCFTCourseNotesCurrentPublic.pdf>.
- [4] H. Nastase, *Introduction to AdS-CFT*, [arXiv:0712.0689](#).
- [5] J. Polchinski and M. J. Strassler, *Hard scattering and gauge / string duality*, *Phys. Rev. Lett.* **88** (2002) 031601, [[hep-th/0109174](#)].
- [6] J. Erlich, E. Katz, D. T. Son, and M. A. Stephanov, *QCD and a holographic model of hadrons*, *Phys. Rev. Lett.* **95** (2005) 261602, [[hep-ph/0501128](#)].
- [7] L. Da Rold and A. Pomarol, *Chiral symmetry breaking from five dimensional spaces*, *Nucl. Phys. B* **721** (2005) 79–97, [[hep-ph/0501218](#)].
- [8] U. Gürsoy and E. Kiritsis, *Exploring improved holographic theories for QCD: Part I*, *JHEP* **02** (2008) 032, [[arXiv:0707.1324](#)].
- [9] U. Gürsoy, E. Kiritsis, and F. Nitti, *Exploring improved holographic theories for QCD: Part II*, *JHEP* **02** (2008) 019, [[arXiv:0707.1349](#)].

- [10] O. Aharony, *A Brief review of 'little string theories'*, *Class. Quant. Grav.* **17** (2000) 929–938, [[hep-th/9911147](#)].
- [11] D. Kutasov, *Introduction to little string theory*, *ICTP Lect. Notes Ser.* **7** (2002) 165–209.
- [12] I. Antoniadis, C. Markou, and F. Rondeau, *Aspects of compactification on a linear dilaton background*, *JHEP* **09** (2021) 137, [[arXiv:2106.15184](#)].
- [13] N. Seiberg, *New theories in six-dimensions and matrix description of M theory on T^{**5} and $T^{**5}/Z(2)$* , *Phys. Lett. B* **408** (1997) 98–104, [[hep-th/9705221](#)].
- [14] M. Berkooz, M. Rozali, and N. Seiberg, *Matrix description of M theory on T^{**4} and T^{**5}* , *Phys. Lett. B* **408** (1997) 105–110, [[hep-th/9704089](#)].
- [15] A. Giveon, N. Itzhaki, and D. Kutasov, $T\bar{T}$ and LST, *JHEP* **07** (2017) 122, [[arXiv:1701.05576](#)].
- [16] G. Giribet, $T\bar{T}$ -deformations, AdS/CFT and correlation functions, *JHEP* **02** (2018) 114, [[arXiv:1711.02716](#)].
- [17] M. Asrat, A. Giveon, N. Itzhaki, and D. Kutasov, *Holography Beyond AdS*, *Nucl. Phys. B* **932** (2018) 241–253, [[arXiv:1711.02690](#)].
- [18] T. Araujo, E. O. Colgáin, Y. Sakatani, M. M. Sheikh-Jabbari, and H. Yavartanoo, *Holographic integration of $T\bar{T} \setminus \mathcal{E} J\bar{T}$ via $O(d, d)$* , *JHEP* **03** (2019) 168, [[arXiv:1811.03050](#)].
- [19] S. Chakraborty, G. Katoch, and S. R. Roy, *Holographic complexity of LST and single trace $T\bar{T}$* , *JHEP* **03** (2021) 275, [[arXiv:2012.11644](#)].
- [20] S. Chakraborty, $\frac{SL(2, \mathbb{R}) \times U(1)}{U(1)}$ CFT, NS5+F1 system and single trace $T\bar{T}$, *JHEP* **03** (2021) 113, [[arXiv:2012.03995](#)].
- [21] S. Georgescu and M. Guica, *Infinite $T\bar{T}$ -like symmetries of compactified LST*, *SciPost Phys.* **16** (2024), no. 1 006, [[arXiv:2212.09768](#)].
- [22] M. Guica, “ $T\bar{T}$ deformations and holography.” <https://indi.to/h333c>.
- [23] C.-K. Chang, C. Ferko, and S. Sethi, *Holography and irrelevant operators*, *Phys. Rev. D* **107** (2023), no. 12 126021, [[arXiv:2302.03041](#)].
- [24] S. Chakraborty, A. Giveon, and D. Kutasov, *Comments on single-trace $T\bar{T}$ holography*, *JHEP* **06** (2023) 018, [[arXiv:2303.12422](#)].
- [25] S. Chakraborty, A. Giveon, and D. Kutasov, *Momentum in Single-trace $T\bar{T}$ Holography*, *Nucl. Phys. B* **998** (2024) 116405, [[arXiv:2304.09212](#)].
- [26] O. Aharony and N. Barel, *Correlation functions in $T\bar{T}$ -deformed Conformal Field Theories*, *JHEP* **08** (2023) 035, [[arXiv:2304.14091](#)].
- [27] S. Fichet, E. Megías, and M. Quirós, *Holography of Linear Dilaton Spacetimes from the Bottom Up*, *Phys. Rev. D* **109** (2024), no. 10 106011, [[arXiv:2309.02489](#)].
- [28] I. Antoniadis, S. Dimopoulos, and A. Giveon, *Little string theory at a TeV*, *JHEP* **05** (2001) 055, [[hep-th/0103033](#)].
- [29] I. Antoniadis, A. Arvanitaki, S. Dimopoulos, and A. Giveon, *Phenomenology of TeV Little String Theory from Holography*, *Phys. Rev. Lett.* **108** (2012) 081602, [[arXiv:1102.4043](#)].
- [30] C. Csáki, G. Lee, S. J. Lee, S. Lombardo, and O. Telem, *Continuum Naturalness*, *JHEP* **03** (2019) 142, [[arXiv:1811.06019](#)].

- [31] E. Megías and M. Quirós, *Gapped Continuum Kaluza-Klein spectrum*, *JHEP* **08** (2019) 166, [[arXiv:1905.07364](#)].
- [32] E. Megías and M. Quirós, *The Continuum Linear Dilaton*, *Acta Phys. Polon. B* **52** (2021) 711, [[arXiv:2104.10260](#)].
- [33] E. Megías and M. Quirós, *Analytical Green’s functions for continuum spectra*, *JHEP* **09** (2021) 157, [[arXiv:2106.09598](#)].
- [34] S. Fichet, E. Megías, and M. Quirós, *Continuum effective field theories, gravity, and holography*, *Phys. Rev. D* **107** (2023), no. 9 096016, [[arXiv:2208.12273](#)].
- [35] S. Fichet, E. Megías, and M. Quirós, *Cosmological dark matter from a bulk black hole*, *Phys. Rev. D* **107** (2023), no. 11 115014, [[arXiv:2212.13268](#)].
- [36] G. ’t Hooft, *Dimensional reduction in quantum gravity*, *Conf. Proc. C* **930308** (1993) 284–296, [[gr-qc/9310026](#)].
- [37] L. Susskind, *The World as a hologram*, *J. Math. Phys.* **36** (1995) 6377–6396, [[hep-th/9409089](#)].
- [38] G. ’t Hooft, *The Holographic principle: Opening lecture*, *Subnucl. Ser.* **37** (2001) 72–100, [[hep-th/0003004](#)].
- [39] R. Bousso, *A Covariant entropy conjecture*, *JHEP* **07** (1999) 004, [[hep-th/9905177](#)].
- [40] R. Bousso, *The Holographic principle*, *Rev. Mod. Phys.* **74** (2002) 825–874, [[hep-th/0203101](#)].
- [41] A. Karch, E. Katz, D. T. Son, and M. A. Stephanov, *Linear confinement and AdS/QCD*, *Phys. Rev. D* **74** (2006) 015005, [[hep-ph/0602229](#)].
- [42] B. Batell and T. Gherghetta, *Dynamical Soft-Wall AdS/QCD*, *Phys. Rev. D* **78** (2008) 026002, [[arXiv:0801.4383](#)].
- [43] P. Colangelo, F. De Fazio, F. Giannuzzi, F. Jugeau, and S. Nicotri, *Light scalar mesons in the soft-wall model of AdS/QCD*, *Phys. Rev. D* **78** (2008) 055009, [[arXiv:0807.1054](#)].
- [44] J. A. Cabrer, G. von Gersdorff, and M. Quirós, *Soft-Wall Stabilization*, *New J. Phys.* **12** (2010) 075012, [[arXiv:0907.5361](#)].
- [45] G. von Gersdorff, *From Soft Walls to Infrared Branes*, *Phys. Rev. D* **82** (2010) 086010, [[arXiv:1005.5134](#)].
- [46] E. Megías and M. Valle, *Singular perturbation theory for the thermodynamic properties of holographic QCD*, *Fortsch. Phys.* **66** (2018), no. 7 1800035, [[arXiv:1707.04747](#)].
- [47] A. F. Faedo, C. Hoyos, M. Piai, R. Rodgers, and J. G. Subils, *Light holographic dilatons near critical points*, *Phys. Rev. D* **110** (2024), no. 12 126017, [[arXiv:2406.04974](#)].
- [48] E. Witten, *Branes and the dynamics of QCD*, *Nucl. Phys. B* **507** (1997) 658–690, [[hep-th/9706109](#)].
- [49] A. Hanany, M. J. Strassler, and A. Zaffaroni, *Confinement and strings in MQCD*, *Nucl. Phys. B* **513** (1998) 87–118, [[hep-th/9707244](#)].
- [50] J. M. Maldacena, *Wilson loops in large N field theories*, *Phys. Rev. Lett.* **80** (1998) 4859–4862, [[hep-th/9803002](#)].
- [51] Y. Kinar, E. Schreiber, and J. Sonnenschein, *Precision ’measurements’ of the Q anti-Q potential in MQCD*, *Nucl. Phys. B* **544** (1999) 633–649, [[hep-th/9809133](#)].

- [52] A. M. Polyakov, *The Wall of the cave*, *Int. J. Mod. Phys. A* **14** (1999) 645–658, [[hep-th/9809057](#)].
- [53] S.-J. Rey and J.-T. Yee, *Macroscopic strings as heavy quarks in large N gauge theory and anti-de Sitter supergravity*, *Eur. Phys. J. C* **22** (2001) 379–394, [[hep-th/9803001](#)].
- [54] O. Andreev and V. I. Zakharov, *Heavy-quark potentials and AdS/QCD*, *Phys. Rev. D* **74** (2006) 025023, [[hep-ph/0604204](#)].
- [55] O. Andreev and V. I. Zakharov, *On Heavy-Quark Free Energies, Entropies, Polyakov Loop, and AdS/QCD*, *JHEP* **04** (2007) 100, [[hep-ph/0611304](#)].
- [56] B. Galow, E. Megías, J. Nian, and H. J. Pirner, *Phenomenology of AdS/QCD and Its Gravity Dual*, *Nucl. Phys. B* **834** (2010) 330–362, [[arXiv:0911.0627](#)].
- [57] N. Horigome and Y. Tanii, *Holographic chiral phase transition with chemical potential*, *JHEP* **01** (2007) 072, [[hep-th/0608198](#)].
- [58] U. Gürsoy, E. Kiritsis, L. Mazzanti, and F. Nitti, *Holography and Thermodynamics of 5D Dilaton-gravity*, *JHEP* **05** (2009) 033, [[arXiv:0812.0792](#)].
- [59] T. Konstandin, G. Nardini, and M. Quirós, *Gravitational Backreaction Effects on the Holographic Phase Transition*, *Phys. Rev. D* **82** (2010) 083513, [[arXiv:1007.1468](#)].
- [60] E. Megías, H. J. Pirner, and K. Veschgini, *QCD thermodynamics using five-dimensional gravity*, *Phys. Rev. D* **83** (2011) 056003, [[arXiv:1009.2953](#)].
- [61] E. Megías, G. Nardini, and M. Quirós, *Cosmological Phase Transitions in Warped Space: Gravitational Waves and Collider Signatures*, *JHEP* **09** (2018) 095, [[arXiv:1806.04877](#)].
- [62] E. Megías, G. Nardini, and M. Quirós, *Gravitational Imprints from Heavy Kaluza-Klein Resonances*, *Phys. Rev. D* **102** (2020), no. 5 055004, [[arXiv:2005.04127](#)].
- [63] E. Megías, G. Nardini, and M. Quirós, *Pulsar timing array stochastic background from light Kaluza-Klein resonances*, *Phys. Rev. D* **108** (2023), no. 9 095017, [[arXiv:2306.17071](#)].
- [64] R. K. Mishra and L. Randall, *Phase transition to RS: cool, not supercool*, *JHEP* **06** (2024) 099, [[arXiv:2401.09633](#)].
- [65] I. R. Klebanov, D. Kutasov, and A. Murugan, *Entanglement as a probe of confinement*, *Nucl. Phys. B* **796** (2008) 274–293, [[arXiv:0709.2140](#)].
- [66] I. Bah, A. Faraggi, L. A. Pando Zayas, and C. A. Terrero-Escalante, *Holographic entanglement entropy and phase transitions at finite temperature*, *Int. J. Mod. Phys. A* **24** (2009) 2703–2728, [[arXiv:0710.5483](#)].
- [67] M. Fujita, T. Nishioka, and T. Takayanagi, *Geometric Entropy and Hagedorn/Deconfinement Transition*, *JHEP* **09** (2008) 016, [[arXiv:0806.3118](#)].
- [68] N. Engelhardt and G. T. Horowitz, *Entanglement Entropy Near Cosmological Singularities*, *JHEP* **06** (2013) 041, [[arXiv:1303.4442](#)].
- [69] S. Chakraborty, A. Giveon, N. Itzhaki, and D. Kutasov, *Entanglement beyond AdS*, *Nucl. Phys. B* **935** (2018) 290–309, [[arXiv:1805.06286](#)].
- [70] M. Fujita, S. He, and Y. Sun, *Thermodynamical property of entanglement entropy and deconfinement phase transition*, *Phys. Rev. D* **102** (2020), no. 12 126019, [[arXiv:2005.01048](#)].

- [71] R. da Rocha, *Holographic entanglement entropy, deformed black branes, and deconfinement in AdS/QCD*, *Phys. Rev. D* **105** (2022), no. 2 026014, [[arXiv:2111.01244](#)].
- [72] N. Jokela, H. Ruotsalainen, and J. G. Subils, *Limitations of entanglement entropy in detecting thermal phase transitions*, *JHEP* **01** (2024) 186, [[arXiv:2310.11205](#)].
- [73] U. Kol, C. Nunez, D. Schofield, J. Sonnenschein, and M. Warschawski, *Confinement, Phase Transitions and non-Locality in the Entanglement Entropy*, *JHEP* **06** (2014) 005, [[arXiv:1403.2721](#)].
- [74] N. Jokela and J. G. Subils, *Is entanglement a probe of confinement?*, *JHEP* **02** (2021) 147, [[arXiv:2010.09392](#)].
- [75] S. Griener, D. E. Kharzeev, and I. Zahed, *Entanglement entropy in a time-dependent holographic Schwinger pair creation*, *Phys. Rev. D* **108** (2023), no. 12 126014, [[arXiv:2310.12042](#)].
- [76] A. Fatemiabhari and C. Nunez, *From conformal to confining field theories using holography*, *JHEP* **03** (2024) 160, [[arXiv:2401.04158](#)].
- [77] J. Abajo-Arastia, J. Aparicio, and E. Lopez, *Holographic Evolution of Entanglement Entropy*, *JHEP* **11** (2010) 149, [[arXiv:1006.4090](#)].
- [78] A. Bagchi, R. Basu, D. Grumiller, and M. Riegler, *Entanglement entropy in Galilean conformal field theories and flat holography*, *Phys. Rev. Lett.* **114** (2015), no. 11 111602, [[arXiv:1410.4089](#)].
- [79] J. Erdmenger, D. Fernandez, M. Flory, E. Megías, A.-K. Straub, and P. Witkowski, *Time evolution of entanglement for holographic steady state formation*, *JHEP* **10** (2017) 034, [[arXiv:1705.04696](#)].
- [80] J. Casalderrey-Solana, C. Ecker, D. Mateos, and W. Van Der Schee, *Strong-coupling dynamics and entanglement in de Sitter space*, *JHEP* **03** (2021) 181, [[arXiv:2011.08194](#)].
- [81] Z. Li, *Holographic entanglement properties in the QCD phase diagram from Einstein-Maxwell-dilaton models*, *Phys. Rev. D* **110** (2024), no. 4 046012, [[arXiv:2402.02944](#)].
- [82] S. Fichet, E. Megías, and M. Quirós, *Holographic fluids from 5D dilaton gravity*, *JHEP* **08** (2024) 077, [[arXiv:2311.14233](#)].
- [83] U. Gürsoy, M. Järvinen, and G. Policastro, *Late time behavior of non-conformal plasmas*, *JHEP* **01** (2016) 134, [[arXiv:1507.08628](#)].
- [84] P. Betzios, U. Gürsoy, M. Järvinen, and G. Policastro, *Quasinormal modes of a strongly coupled nonconformal plasma and approach to criticality*, *Phys. Rev. D* **97** (2018), no. 8 081901, [[arXiv:1708.02252](#)].
- [85] P. Betzios, U. Gürsoy, M. Järvinen, and G. Policastro, *Fluctuations in a nonconformal holographic plasma at criticality*, *Phys. Rev. D* **101** (2020), no. 8 086026, [[arXiv:1807.01718](#)].
- [86] U. Gürsoy, M. Järvinen, G. Policastro, and N. Zinnato, *Analytic long-lived modes in charged critical plasma*, *JHEP* **06** (2022) 018, [[arXiv:2112.04296](#)].
- [87] C. Csaki, *TASI lectures on extra dimensions and branes*, in *From fields to strings: Circumnavigating theoretical physics. Ian Kogan memorial collection (3 volume set)*, pp. 605–698, 2004. [hep-ph/0404096](#). [[967\(2004\)](#)].

- [88] R. Sundrum, *Effective field theory for a three-brane universe*, *Phys. Rev.* **D59** (1999) 085009, [[hep-ph/9805471](#)].
- [89] R. Sundrum, *Compactification for a three-brane universe*, *Phys. Rev.* **D59** (1999) 085010, [[hep-ph/9807348](#)].
- [90] J. Polchinski, *Tasi lectures on D-branes*, in *Fields, strings and duality. Proceedings, Summer School, Theoretical Advanced Study Institute in Elementary Particle Physics, TASI'96, Boulder, USA, June 2-28, 1996*, pp. 293–356, 1996. [hep-th/9611050](#).
- [91] C. P. Bachas, *Lectures on D-branes*, in *Duality and supersymmetric theories. Proceedings, Easter School, Newton Institute, Euroconference, Cambridge, UK, April 7-18, 1997*, pp. 414–473, 1998. [hep-th/9806199](#).
- [92] M. J. Duff, *Supermembranes*, in *26th British Universities Summer School in Theoretical Elementary Particle Physics (BUSSTEPP 1996) Swansea, Wales, September 3-18, 1996*, 1996. [hep-th/9611203](#).
- [93] T. Shiromizu, K.-i. Maeda, and M. Sasaki, *The Einstein equation on the 3-brane world*, *Phys. Rev. D* **62** (2000) 024012, [[gr-qc/9910076](#)].
- [94] W. Israel, *Singular hypersurfaces and thin shells in general relativity*, *Nuovo Cim. B* **44S10** (1966) 1. [Erratum: *Nuovo Cim.B* 48, 463 (1967)].
- [95] D. Langlois, L. Sorbo, and M. Rodriguez-Martinez, *Cosmology of a brane radiating gravitons into the extra dimension*, *Phys. Rev. Lett.* **89** (2002) 171301, [[hep-th/0206146](#)].
- [96] D. Langlois and L. Sorbo, *Bulk gravitons from a cosmological brane*, *Phys. Rev. D* **68** (2003) 084006, [[hep-th/0306281](#)].
- [97] C. Csaki, M. L. Graesser, and G. D. Kribs, *Radion dynamics and electroweak physics*, *Phys. Rev. D* **63** (2001) 065002, [[hep-th/0008151](#)].
- [98] A. Hebecker and J. March-Russell, *Randall-Sundrum II cosmology, AdS / CFT, and the bulk black hole*, *Nucl. Phys. B* **608** (2001) 375–393, [[hep-ph/0103214](#)].
- [99] G. K. Karananas, A. Kehagias, and J. Taskas, *Islands in linear dilaton black holes*, *JHEP* **03** (2021) 253, [[arXiv:2101.00024](#)].
- [100] S. S. Gubser, *Curvature singularities: The Good, the bad, and the naked*, *Adv. Theor. Math. Phys.* **4** (2000) 679–745, [[hep-th/0002160](#)].
- [101] Y. Kinar, E. Schreiber, and J. Sonnenschein, *Q anti-Q potential from strings in curved space-time: Classical results*, *Nucl. Phys. B* **566** (2000) 103–125, [[hep-th/9811192](#)].
- [102] E. S. Fradkin and A. A. Tseytlin, *Quantum String Theory Effective Action*, *Nucl. Phys. B* **261** (1985) 1–27. [Erratum: *Nucl.Phys.B* 269, 745–745 (1986)].
- [103] C. G. Callan, Jr., E. J. Martinec, M. J. Perry, and D. Friedan, *Strings in Background Fields*, *Nucl. Phys. B* **262** (1985) 593–609.
- [104] C. Lovelace, *Stability of String Vacua. 1. A New Picture of the Renormalization Group*, *Nucl. Phys. B* **273** (1986) 413–467.
- [105] A. F. Faedo, D. Mateos, D. Pravos, and J. G. Subils, *Mass Gap without Confinement*, *JHEP* **06** (2017) 153, [[arXiv:1702.05988](#)].
- [106] J. H. Schwarz, *Superstring Theory*, *Phys. Rept.* **89** (1982) 223–322.

- [107] M. B. Green, J. H. Schwarz, and E. Witten, *Superstring Theory Vol. 2: Loop Amplitudes, Anomalies and Phenomenology*. Cambridge University Pr., 7, 1988.
- [108] D. Chialva, *String Mass Shifts*, *Nucl. Phys. B* **819** (2009) 225–255, [[arXiv:0903.3979](#)].
- [109] S. Ryu and T. Takayanagi, *Holographic derivation of entanglement entropy from AdS/CFT*, *Phys. Rev. Lett.* **96** (2006) 181602, [[hep-th/0603001](#)].
- [110] T. Nishioka, S. Ryu, and T. Takayanagi, *Holographic Entanglement Entropy: An Overview*, *J. Phys. A* **42** (2009) 504008, [[arXiv:0905.0932](#)].
- [111] H. Casini, M. Huerta, and R. C. Myers, *Towards a derivation of holographic entanglement entropy*, *JHEP* **05** (2011) 036, [[arXiv:1102.0440](#)].
- [112] M. Headrick, *General properties of holographic entanglement entropy*, *JHEP* **03** (2014) 085, [[arXiv:1312.6717](#)].
- [113] D. D. Blanco, H. Casini, L.-Y. Hung, and R. C. Myers, *Relative Entropy and Holography*, *JHEP* **08** (2013) 060, [[arXiv:1305.3182](#)].
- [114] V. E. Hubeny, H. Maxfield, M. Rangamani, and E. Tonni, *Holographic entanglement plateaux*, *JHEP* **08** (2013) 092, [[arXiv:1306.4004](#)].
- [115] T. Faulkner, A. Lewkowycz, and J. Maldacena, *Quantum corrections to holographic entanglement entropy*, *JHEP* **11** (2013) 074, [[arXiv:1307.2892](#)].
- [116] A. Lewkowycz and J. Maldacena, *Generalized gravitational entropy*, *JHEP* **08** (2013) 090, [[arXiv:1304.4926](#)].
- [117] T. Barrella, X. Dong, S. A. Hartnoll, and V. L. Martin, *Holographic entanglement beyond classical gravity*, *JHEP* **09** (2013) 109, [[arXiv:1306.4682](#)].
- [118] N. Engelhardt and A. C. Wall, *Quantum Extremal Surfaces: Holographic Entanglement Entropy beyond the Classical Regime*, *JHEP* **01** (2015) 073, [[arXiv:1408.3203](#)].
- [119] C. T. Asplund, A. Bernamonti, F. Galli, and T. Hartman, *Holographic Entanglement Entropy from 2d CFT: Heavy States and Local Quenches*, *JHEP* **02** (2015) 171, [[arXiv:1410.1392](#)].
- [120] A. Almheiri, X. Dong, and B. Swingle, *Linearity of Holographic Entanglement Entropy*, *JHEP* **02** (2017) 074, [[arXiv:1606.04537](#)].
- [121] D. Neuenfeld, *Homology conditions for RT surfaces in double holography*, *Class. Quant. Grav.* **39** (2022), no. 7 075009, [[arXiv:2105.01130](#)].
- [122] M. Jarvinen and D. Weissman, *Black hole effective theory for strongly interacting matter*, *Phys. Rev. D* **111** (2025), no. 2 L021903, [[arXiv:2405.17553](#)].
- [123] R. B. Mann and R. McNees, *Boundary Terms Unbound! Holographic Renormalization of Asymptotically Linear Dilaton Gravity*, *Class. Quant. Grav.* **27** (2010) 065015, [[arXiv:0905.3848](#)].
- [124] E. Megías, M. Pérez-Victoria, and M. Quirós, *Undecay*, *JHEP* **05** (2024) 158, [[arXiv:2310.16593](#)].
- [125] P. Creminelli, A. Nicolis, and R. Rattazzi, *Holography and the electroweak phase transition*, *JHEP* **03** (2002) 051, [[hep-th/0107141](#)].
- [126] U. Gürsoy, *Continuous Hawking-Page transitions in Einstein-scalar gravity*, *JHEP* **01** (2011) 086, [[arXiv:1007.0500](#)].

- [127] D. Elander, A. F. Faedo, D. Mateos, and J. G. Subils, *Phase transitions in a three-dimensional analogue of Klebanov-Strassler*, *JHEP* **06** (2020) 131, [[arXiv:2002.08279](#)].
- [128] S. S. Gubser, I. R. Klebanov, and A. M. Polyakov, *Gauge theory correlators from noncritical string theory*, *Phys. Lett.* **B428** (1998) 105–114, [[hep-th/9802109](#)].
- [129] P. Baratella, A. Pomarol, and F. Rompineve, *The Supercooled Universe*, *JHEP* **03** (2019) 100, [[arXiv:1812.06996](#)].
- [130] S. J. Lee, Y. Nakai, and M. Suzuki, *Multiple hierarchies from a warped extra dimension*, *JHEP* **02** (2022) 050, [[arXiv:2109.10938](#)].